

Antiferro Quadrupole Orders in Non-Kramers Doublet Systems

Kazumasa HATTORI^{1,2*} and Hirokazu TSUNETSUGU¹

¹*Institute for Solid State Physics, University of Tokyo, 5-1-5, Kashiwanoha, Kashiwa, Chiba 277-8581, Japan*

²*Institut für Theoretische Physik, Universität zu Köln, Zùlpicher Str., 77, D-50937 Köln, Germany*

We investigate antiferro quadrupole orders in systems with non-Kramers doublet ground state with total angular momentum $J = 4$ in T_d point group symmetry. We demonstrate that a pure O_2^2 antiferro quadrupole order is impossible in general crystalline-electric field potential and should be accompanied by ferro O_2^0 quadrupole moment. The temperature and magnetic-field phase diagram is obtained by mean-field approximation of intersite quadrupole interactions and the excitation spectrum is analyzed by “spin”-wave approximations. Gapless excitations emerge at the boader of antiferro O_2^2 quadrupole phases under magnetic field. Quadrupole susceptibilities in the antiferro quadrupole ordered state exhibit unusual singularity and especially the uniform quadrupole susceptibility diverges in addition to the staggered ones. These unusual singularities are also realized at the critical field along [111] direction. We also discuss recent experimental results in $\text{PrT}_2\text{X}_{20}$ ($T=\text{Ir, Rh, Ti, V}$, and $X=\text{Zn, Al}$).

1. Introduction

Orbital order appears in varieties of systems in condensed matter physics such as in d - and f -electron strongly correlated systems with orbital degrees of freedom.^{1,2)} Quadrupole orders are typical and most intensively studied cases. Such orbital orders can be in principle described by similar theoretical approaches as in spin systems. As is evident from the nature of orbital degrees of freedom, interactions have spatial anisotropies depending on what kinds of orbital is considered and the symmetry is in general not fully isotropic in the orbital space. These differ from the typical case of spin systems, where the spin anisotropy is zero or not so strong unless the spin-orbit interaction is very strong. Each orbital order possesses a unique property and exploring such uniqueness is an important issue of the condensed matter theories and experiments.

Recently, Pr-based compounds $\text{PrT}_2\text{X}_{20}$ ($T=\text{Ir, Rh, Ti, V}$, and $X=\text{Zn, Al}$), so-called 1-2-20 compounds, have attracted great attention.^{3–12)} In these compounds, each Pr ion has $(4f)^2$ electron configuration. Its ground state under the crystalline electric field (CEF) is a non-Kramers doublet,¹³⁾ and this doublet couples with conduction electrons. This is a typical situation that the two-channel Kondo effects take place. Thus, it is expected that these compounds show exotic properties due to the two-channel Kondo effects.⁶⁾ Nevertheless, the doublet is not completely screened and all the compounds exhibit an orbital order below ~ 1 K. Surprisingly, some of them show even superconductivity at very low temperature in the ordered phase.^{3, 5, 7, 8)}

Since the first-excited CEF multiplet is located at ~ 30 K^{3–5, 13, 14)} and the phase transition occurs at ~ 1 K, it is likely that the phase transition in the 1-2-20 compounds

is about the degrees of freedom in the ground-state multiplet, *i.e.*, an ordering of the non-Kramers doublets. The ground-state non-Kramers doublet is denoted as Γ_3 according to the standard notation of irreducible representations (irreps) of T_d group.¹⁵⁾ Within the Γ_3 doublet states, two quadrupole operators and one octupole operator have finite matrix elements. The former belong to Γ_3 irrep, while the latter Γ_2 . Thus, the (local) order parameter of the orbital order is either Γ_3 quadrupole or otherwise Γ_2 octupole. There has been no direct evidence for which type of order is realized, but results of the neutron scattering¹⁴⁾ and the ultrasound experiments^{10, 11)} suggest a quadrupole order and no evidence for octupole or magnetic dipole order has been observed so far.

Quadrupole orders were intensively discussed for f -electron system CeB_6 .^{2, 16, 17)} and another example TmTe .^{18, 19)} The CEF ground state of Ce (Tm) ion is the Γ_8 quartet in O_h symmetry, where it has a $4f^1(4f^{13})$ electron configuration in contrast to the case of the Pr 1-2-20 compounds. Despite this difference, they also exhibit a quadrupole order. On the basis of a localized model, the results by mean-field approximations are qualitatively consistent with the experimental ones.^{16, 19)} Several other systems also have a non-Kramers Γ_3 doublet ground state, and PrPb_3 ,²⁰⁾ PrInAg_2 ,²¹⁾ and PrMg_3 ²²⁾ are examples. In the previous studies, experimental group tried fitting their experimental data by a mean-field approximation of the CEF model, for example, in $\text{PrRh}_2\text{Zn}_{20}$,⁵⁾ PrPb_3 ,²³⁾ and $\text{PrIr}_2\text{Zn}_{20}$.²⁴⁾ In this paper, we extend their analysis and provide detailed theoretical account of Γ_3 quadrupole ordering. We have also discovered unusual properties related to this order and unveiled their origin.

The main purpose of this paper is to provide a basic understanding of the Γ_3 quadrupole order and the

*E-mail: hattori@issp.u-tokyo.ac.jp

nature of its transition, rather than to make quantitative comparisons with experimental data. Various points need careful analysis. These include (i) constraints on quadrupole ordered states by general arguments, (ii) excitation spectra in ordered states, and (iii) unusual criticality even within mean-field approximation. To this end, we employ the simplest model for inter-site interaction relevant to the quadrupole order and ignore all other interactions that might be present in the real systems.

In this paper, we will carry out a detailed theoretical analysis on the Γ_3 quadrupole order in a diamond-lattice model with a minimal quadrupole-quadrupole interaction on the basis of the CEF level scheme relevant to $\text{PrIr}_2\text{Zn}_{20}$ as an example. The model shows quadrupole anisotropy and this is general for the Γ_3 degrees of freedom in cubic symmetry. We will discuss it in detail, and determine and examine the mean-field phase diagram in Sect. 2. We will then in Sect. 3 study excitation spectra based on spin-wave type approximations and clarify unusual critical behaviors found in this system. In Sect. 4, we will discuss some experimental results of the 1-2-20 compounds. We will also study possible couplings of quadrupoles with other degrees of freedom including other multipole moments and phonons. Section 5 is a summary of the present paper.

2. A Basic Model and Mean-field Approximation

In this section, we will first discuss the effect of single-ion anisotropy and its effect on quadrupole orders. Then, we will analytically analyze the mean-field ground state for zero magnetic field. In the final part of this section, we will show numerical results and discuss the temperature vs. magnetic-field phase diagram.

2.1 Crystalline-electric-field Hamiltonian

We start with investigating a CEF model. Each Pr ion has total angular momentum $J = 4$ and feels the CEF with the local T_d point group symmetry. The CEF states are represented by the irreps of the T_d group. The nine states in the $J = 4$ multiplet are splitted by the CEF as shown by

$$H_{\text{CEF}} = \sum_i \left\{ \epsilon_2 |\mathbf{Q}(i)|^2 - \epsilon_3 \left[Q_z^3(i) - 3\overline{Q_z(i)Q_x^2(i)} \right] \right\}. \quad (1)$$

Here, $\epsilon_{2,3}$ are constants and $\mathbf{Q}(i)$ is the quadrupolar operator at the site i which is represented by the Stevens operators²⁵⁾ as $\mathbf{Q}(i) = (Q_z(i), Q_x(i)) = (O_2^0(i), \sqrt{3}O_2^2(i))/8$. In terms of dipole operators $J_{x,y,z}(i)$ for the $J = 4$ manifold, $O_2^0(i) = 2J_z^2(i) - J_x^2(i) - J_y^2(i)$ and $O_2^2(i) = J_x^2(i) - J_y^2(i)$. The $\overline{AB^2}$ denotes a cyclic permutation of three operators: $\overline{AB^2} \equiv AB^2 + BAB + B^2A$. With this normalization, the operator $\mathbf{Q}(i)$ within the Γ_3 subspace is represented by the two Pauli matrices $\mathbf{Q} \sim (\tau_z, -\tau_x)$ with the basis states listed in Appendix A. The relation between Eq. (1) and the conventional

form of the CEF Hamiltonian (B.1) is summarized in Appendix B. The advantage in using Eq. (1) is that one can easily understand the single-ion anisotropy in the quadrupole sector.

2.2 Single-site anisotropy and quadrupole ordering

The CEF Hamiltonian (1) readily indicates that the anisotropic ϵ_3 term affects the quadrupole order parameters Q_z and Q_x *differently*. This is related to the existence of Z_3 symmetry in \mathbf{Q} space. We can rewrite the ϵ_3 term in Eq. (1) as

$$Q_z^3 - 3\overline{Q_z Q_x^2} = \frac{4}{3} \sum_{l=0}^2 Q_l^3, \quad (2)$$

where we have omitted the site index i and $Q_l = \mathbf{n}_l \cdot \mathbf{Q}$ with $\mathbf{n}_l = (\cos 2l\pi/3, \sin 2l\pi/3)$. Any symmetry operations in cubic groups are reduced to permutations of (lmn) in the Q_l space with $0 \leq l, m, n \leq 2$. There exists an essential difference between Q_z and Q_x . The inversion $Q_x \rightarrow -Q_x$ corresponds to the exchange of Q_1 and Q_2 and this is a symmetry operation of H_{CEF} . However, the inversion $Q_z \rightarrow -Q_z$ is not a symmetry operation. This is evident from the fact that the ϵ_3 term contains odd numbers of Q_z .

To understand this point more intuitively, we map the ϵ_3 term to a classical one. This leads

$$Q_z^3 - 3\overline{Q_z Q_x^2} \rightarrow Q^3 \cos 3\theta, \quad (3)$$

where we have introduced the polar coordinates $\mathbf{Q} = Q[\cos \theta, \sin \theta]$.²⁶⁾ Thus, it is apparent that θ and $-\theta$ are equivalent in energy, while θ and $\pi - \theta$ is inequivalent as shown in Fig. 1.²⁷⁾

This anisotropy in \mathbf{Q} -space imposes an important constraint on the symmetry of quadrupole ordering. We will study this ordering in detail in Sect. 2.3, but now briefly discuss the constraint due to the anisotropy. The most important point is the impossibility of a pure antiferro Q_x (O_2^2) order, $\langle \mathbf{Q}(i) \rangle = (0, \pm Q)$ unless the Hamiltonian is finely tuned. This state is *unstable* because of the ϵ_3 term. The single-ion anisotropy H_{CEF} favors the three directions in the \mathbf{Q} space: $\theta = 2l\pi/3$ ($l = 0, 1, 2$) for $\epsilon_3 > 0$ and $\theta = (2l + 1)\pi/3$ for $\epsilon_3 < 0$. Thus, a uniform $\langle Q_z \rangle$ is induced, and its sign is determined by the sign of the anisotropy energy ϵ_3 . When $\epsilon_3 > 0$, $\langle Q_z \rangle < 0$, while $\langle Q_z \rangle > 0$ when $\epsilon_3 < 0$. In contrast to the antiferro Q_x order, a pure antiferro or ferri Q_z (O_2^0) order is possible; $\langle \mathbf{Q}(i) \rangle = (Q, 0), (-Q', 0)$. Note, however, that, when $\epsilon_3 < 0$, the the ground state of H_{CEF} is not Γ_3 . Although this argument is based on the classical mapping (3), the result is valid for the quantum Hamiltonian as will be discussed in Sect. 2.4, where we will see similar anisotropic term appears in the free energy and in the ground-state energy.

The difference between Q_x and Q_z orderings discussed above becomes clearer if one notices the *real* symmetry in the \mathbf{Q} space. As the energy landscape in Fig. 1 shows, the

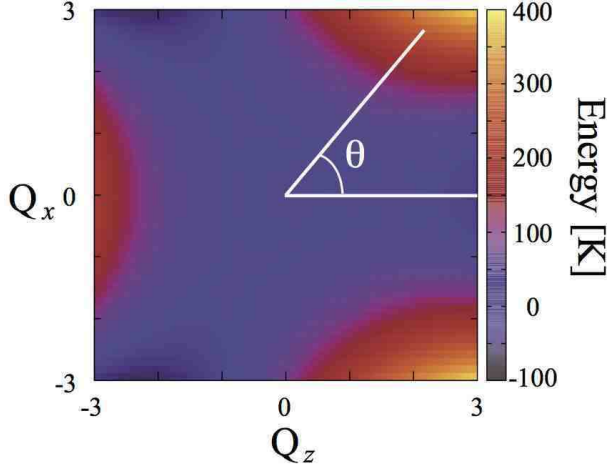


Fig. 1. (Color online) Classical potential energy (single-ion anisotropy) due to Eq. (1) in the quadrupolar space with $\epsilon_2 = 9.709$ K and $\epsilon_3 = 4.088$ K.

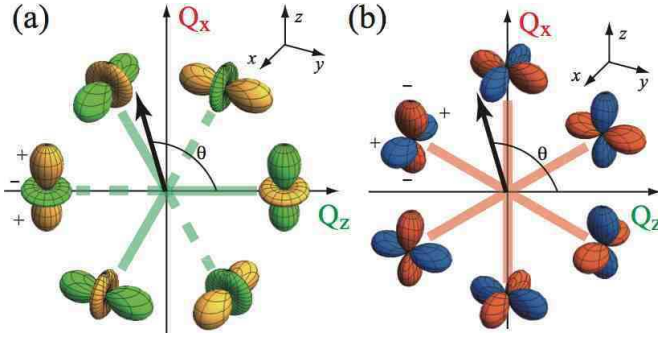


Fig. 2. (Color online) Quadrupole order parameters in Q_z - Q_x plane for (a) O_2^+ type and (b) O_2^- type. \pm indicates the sign of the charge distribution. Note that the shapes of order parameters shown do not reflect the real charge density of f-electron orbitals, but just represent the symmetry of Γ_3 irreps.

\mathbf{Q} order parameter space has the trigonal symmetry Z_3 , not the continuous $O(2)$ symmetry. Any quadrupole ordering is actually the breaking of this Z_3 symmetry. The three-fold symmetry (Z_3) represents the equivalence of the three (x, y, z) principle axes of quadrupole moments in real space.

To understand this, it is instructive to show the types of quadrupole order parameter in the two-dimensional \mathbf{Q} space. Figure 2 illustrates shapes of quadrupole moments in the \mathbf{Q} space. Namely $\theta = 0, 2\pi/3$, and $4\pi/3$ correspond to quadrupole moments with $(3z^2 - r^2)$, $(3x^2 - r^2)$, and $(3y^2 - r^2)$, respectively, with $\theta + \pi$ corresponding to those with opposite sign and $r^2 = x^2 + y^2 + z^2$. Similarly, those for $(x^2 - y^2)$, $(y^2 - z^2)$ and $(z^2 - x^2)$ are at $\theta = \pi/2, 7\pi/6$, and $11\pi/6$, respectively with opposite sign for $\theta + \pi$.

2.3 A model for the Pr 1-2-20 compounds

The model we discuss throughout this paper includes only degrees of freedom of localized f-electrons with

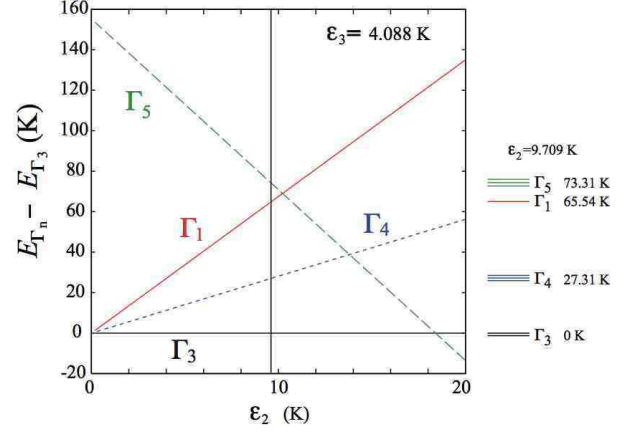


Fig. 3. (Color online) Single-ion energy level scheme determined by H_{CEF} for $\epsilon_3 = 4.088$ K. Vertical line represents $\epsilon_2 = 9.709$ K and the energy scheme there is shown in the right.

quadrupole-quadrupole exchange interaction under zero or finite magnetic field. Although quite simplified, this is a natural model to qualitatively describe essential aspects of the Pr-based 1-2-20 compounds. The transition temperature of the unidentified order in these systems is below 1 K, while the lowest CEF level above the Γ_3 ground state has the excitation energy of ~ 30 K.^{3-5,13,14} This indicates that the doublet ground states play a dominant role in this transition. In the Γ_3 doublet, quadrupole and octupole moments are the only active operators. Therefore, their orderings are the most natural candidate of the transition. For example, a quadrupole order is suggested by anomaly observed in ultrasound experiments, and they also show that the inter-site quadrupole-quadrupole interaction is antiferro for $\text{PrIr}_2\text{Zn}_{20}$ ¹⁰ and $\text{PrRh}_2\text{Zn}_{20}$.¹¹ For $\text{PrTi}_2\text{Al}_{20}$, the quadrupole interaction is ferro²⁸ and this is also consistent with the neutron scattering experiments.¹⁴ These strongly suggest that the transition is an ordering of these quadrupoles, and thus, we investigate this case in detail in this paper.

Concerning inter-site interactions, there also exist some magnetic exchange interactions, which excite the Γ_3 ground state to Γ_4 and Γ_5 levels. They may modify, for example, the details of the temperature-magnetic field phase diagram, but the essential part of all the properties in this transition is described by our minimal model. In this paper, we concentrate on analyzing the simplest model with quadrupole exchange interactions defined as

$$H = H_{\text{CEF}} + \lambda \sum_{\langle i,j \rangle} \mathbf{Q}(i) \cdot \mathbf{Q}(j) - \mu \sum_i \mathbf{H} \cdot \mathbf{J}(i). \quad (4)$$

Here, we consider this Hamiltonian on the diamond lattice of Pr sites. $\mathbf{J}(i) = (J_x(i), J_y(i), J_z(i))$ represents the magnetic dipole operator at the site i . When the magnetic field \mathbf{H} is applied, it couples with \mathbf{J} . Here, the coupling constant is the “magnetic moment” (more precisely,

gyromagnetic constant) μ , and $\mu = g\mu_B$ with $g = 4/5$ for $J = 4$ multiplet and μ_B being the Bohr magneton. The quadrupole-quadrupole interaction λ is set to $\lambda > 0$, *i.e.*, antiferro, and the summation is over nearest-neighbor pairs. Although a ferro quadrupole order is suggested in PrTi₂Al₂₀,⁶⁾ we do not discuss the case for $\lambda < 0$ in detail in this paper. Some comments on ferro quadrupole orders will be given in Sect. 4.1.

For ϵ_2 and ϵ_3 in H_{CEF} , we choose the representative values for the 1-2-20 compounds similar to those determined by inelastic neutron scattering experiments for PrIr₂Zn₂₀:¹³⁾ $\epsilon_2 = 9.709$ K and $\epsilon_3 = 4.088$ K. This leads CEF level scheme shown in Fig. 3: $E_3 = 0$ K, $E_4 = 27.31$ K, $E_1 = 65.54$ K, $E_5 = 73.31$ K. The CEF level scheme with fixed $\epsilon_3 = 4.088$ K is plotted as a function of ϵ_2 in Fig. 3, where we show the part where the ground state is Γ_3 doublet.

It should be noted that conduction electrons in the 1-2-20 compounds is not taken into account in Eq. (4). We do not discuss the Kondo physics or other properties originating from coupling with conduction electrons.^{6,7)} One may regard our localized model as a renormalized effective one after tracing out the conduction electrons. It is natural to expect that this simplification is not serious if one considers symmetry breakings of local moments as shown in earlier works.^{16,17,19)}

It would be helpful to present one of our main results before explaining details of analysis. It is the mean-field phase diagram in the parameter space of temperature T and magnetic field \mathbf{H} . Figure 4 shows the results for \mathbf{H} along three high-symmetry directions. In the followings, we will discuss the nature of each phase in details.

2.4 Analysis of ground state for zero magnetic field

In this subsection, we investigate the ground state for $\mathbf{H} = \mathbf{0}$ by a mean-field approximation. For $\mathbf{H} = \mathbf{0}$, relevant Hilbert space at one site is reduced to three states, Γ_3 doublet and Γ_1 singlet. The other states are decoupled since there are no quadrupole matrix elements between $\Gamma_{1,3}$ states and $\Gamma_{4,5}$ states, and thus, we can safely neglect them.

As shown in Appendix C, the ground-state energy is given by Eq. (C.7). We want to search for small $z\lambda/E_1$ a solution that minimizes Eq. (C.7). Here, z is the number of the nearest-neighbor sites ($z = 4$ for the diamond lattice). In the limit of $E_1 \rightarrow \infty$, the moment modulus $|\langle \mathbf{Q} \rangle|$ approaches 1 on A and B sites, and the anisotropy energy vanishes. Therefore, in this limit, any antiferro quadrupole order $\langle \mathbf{Q}^B \rangle = -\langle \mathbf{Q}^A \rangle$ with $|\langle \mathbf{Q}^{A,B} \rangle| = 1$ is the ground state irrespective of the direction of $\langle \mathbf{Q}^{A,B} \rangle$. Here, we refer to this order as ‘‘antiferro,’’ but note that the ordering wave vector is $\mathbf{q} = \mathbf{0}$. This is because the unit cell of the diamond lattice contains both A and B sublattices. This degeneracy is lifted in the order of $(z\lambda/E_1)^3$ as we will show below. When $z\lambda/E_1$ is finite but small, $|\langle \mathbf{Q}^{A(B)} \rangle| = 1 + \delta q^{A(B)}$, $\theta_A = \theta + \delta\theta$ and

$\theta_B = \theta + \pi - \delta\theta$. $\delta\theta$ represents the deformation of the antiparallel alignment of $\langle \mathbf{Q}^A \rangle$ and $\langle \mathbf{Q}^B \rangle$, which will turn out to be important. To explicitly show the anisotropic term in the energy, we minimize this energy with respect to δq^A , δq^B and $\delta\theta$ for a given value of θ . In the leading order, the optimized values of the parameters are

$$(\delta q^A, \delta q^B) \simeq \frac{35}{2} \left(\cos^2 \frac{3\theta}{2}, \sin^2 \frac{3\theta}{2} \right) \left(\frac{z\lambda}{E_1} \right), \quad (5)$$

$$\delta\theta \simeq -\frac{105}{16} \sin 3\theta \left(\frac{z\lambda}{E_1} \right). \quad (6)$$

Higher order corrections in Eqs. (5) and (6) affect the ground-state energy (C.7) in the order $(z\lambda/E_1)^5$, and thus can be safely neglected. Using Eqs. (5) and (6), we obtain

$$\begin{aligned} \frac{E_{\text{mf}}^{\text{gs}}}{E_1} &= -\left(\frac{z\lambda}{E_1} \right) - \frac{35}{4} \left(\frac{z\lambda}{E_1} \right)^2 \\ &+ \frac{35}{256} \left(29 + 35 \cos 6\theta \right) \left(\frac{z\lambda}{E_1} \right)^3 + \dots \end{aligned} \quad (7)$$

From Eq. (7), one can see that $\partial E_{\text{mf}}^{\text{gs}}/\partial\theta = 0$ at $\theta = n\pi/6$ with n being integers and these values of θ correspond to the order parameters depicted in Figs. 2(a) and (b). For sufficiently small $z\lambda/E_1$, odd n solutions [Fig. 2(b)] have a lower energy than even n solutions, and thus the ground state is six-fold degenerate with $|\langle \mathbf{Q}^A \rangle| = |\langle \mathbf{Q}^B \rangle|$. The primary order parameter is antiferro quadrupole of $Q_x(O_2^2)$ type, and as discussed in Sect. 2.2, this is generally accompanied by ferro quadrupole of $Q_z(O_2^0)$. This is similar to the case of parasite ferromagnetism in antiferromagnets with Dzyaloshinskii-Moriya interaction. The amplitude of the parasite Q_z moment is determined by the deformation angle, $\delta\theta$ between \mathbf{Q}^A and \mathbf{Q}^B . It is small and of the order $z\lambda/E_1$, whereas the amplitude of primary order parameter is $|Q_x| \sim 1$.

The six-fold degeneracy of the ground state is due to $Z_3 \otimes Z_2$ symmetry of the lattice. Z_3 symmetry is about the equivalence of the three principle axes (x, y, z). Z_2 is the symmetry between the two sublattices. The emergence of the secondary order in the Q_z component is consistent with the analysis based on the single-site CEF anisotropy discussed in Sect. 2.2.

When the intersite coupling λ increases, the quadrupole order in the ground state changes from the Q_x antiferro order to the Q_z antiferro order through a first-order transition. One can see this behavior in the fact that the $\cos 6\theta$ term in the variational energy (7) has a negative coefficient in the order $(z\lambda/E_1)^4$, *i.e.*, the sign is opposite to that in the leading order $(z\lambda/E_1)^3$. To examine the change in $\langle \mathbf{Q}^{A,B} \rangle$ quantitatively, we have numerically solved the mean-field equations and found that the transition occurs at $z\lambda/E_1 \sim 0.0375$.

2.5 Non-linear Zeeman term for quadrupole moments

Let us briefly discuss effects of magnetic fields on Γ_3 degrees of freedom. For small magnetic field, its coupling

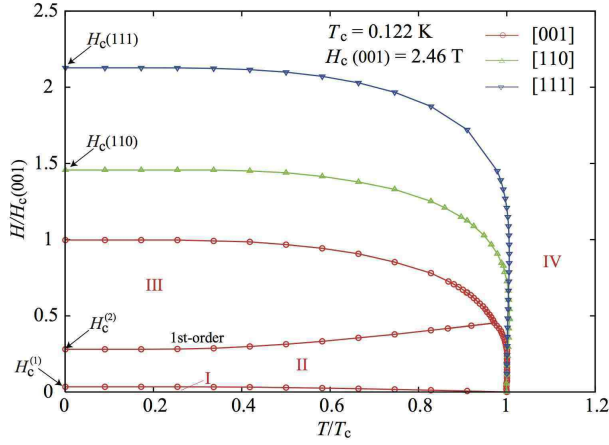


Fig. 4. (Color online) Temperature-magnetic field phase diagram for $\mathbf{H} \parallel [001]$, $[110]$, and $[111]$.

to the quadrupole is calculated by the second-order perturbation in \mathbf{H} , in which the intermediate virtual states are excited magnetic Γ_4 and Γ_5 states, and is given as

$$H_Q = -\alpha \left[(2H_z^2 - H_x^2 - H_y^2)Q_z + \sqrt{3}(H_x^2 - H_y^2)Q_x \right], \quad (8)$$

$$\alpha = \mu^2 \left(\frac{7}{3E_4} - \frac{1}{E_5} \right), \quad (9)$$

where $\alpha > 0$ for our choice of the CEF level scheme. This coupling leads to the effects of applied magnetic field on quadrupole orders.

Related to the cubic crystal symmetry or equivalently Z_3 symmetry in the \mathbf{Q} -space for $\mathbf{H} = \mathbf{0}$, there exist three equivalent ordered states, and they form a multi-domain structure. These three states correspond to the angle $\theta = \pi/2, 7\pi/6$, and $11\pi/6$. Magnetic field \mathbf{H} favors some of the three domains and disfavor the others, depending on the field direction, and thus controls the domain structure. When $\mathbf{H} \parallel [110]$, the domain of $\theta = \pi/2$ is favored. This domain corresponds to $\sim (x^2 - y^2)$ state. In a similar way, for $\mathbf{H} \parallel [001]$ two domains $\theta = 7\pi/6 : (y^2 - z^2)$ and $11\pi/6 : (z^2 - x^2)$ are selected, since the magnetic field favors positive Q_z . For $[111]$ direction, the quadratic terms in (8) vanishes and the leading effect is the coupling to octupole, $\sim H_x H_y H_z T_{xyz}$. Thus, T_{xyz} octupole moment is induced for $\mathbf{H} \parallel [111]$ direction, where the degeneracy of the three domains of Q_x -type antiferro quadrupole states is not lifted.

Note that the above discussions do not include the contribution of induced magnetic multipoles that originates from the hybridization between Γ_3 and the excited states. When the magnetic field is weak, the induced magnetic parts do not play important roles in selecting domains and the direct effects in the Γ_3 sector dominates.

2.6 Temperature-magnetic field phase diagram

In this subsection, we will discuss the T - H phase diagram shown in Fig. 4 in details and generalize the anal-

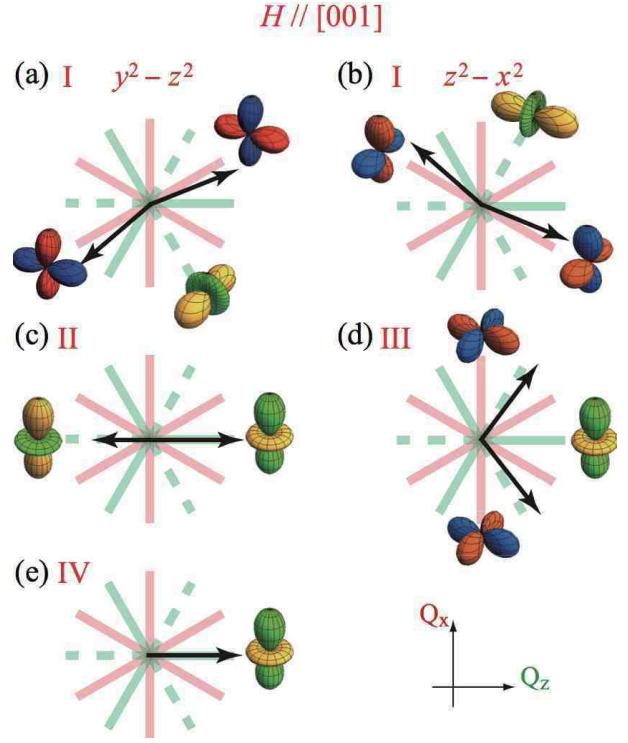


Fig. 5. (Color online) Schematic pictures of quadrupole orders for $\mathbf{H} \parallel [001]$. (a) and (b) two domains for phase-I. (c) Q_z antiferro quadrupole state in phase-II. (d) canted state for phase-III. (e) high-field polarized state.

ysis in the previous subsection. To this end, we study the full model (4). The phase diagram shows several ordered phases under magnetic field and we will examine the nature of these phases.

Figure 4 shows T - H phase diagrams determined by the mean-field analysis and \mathbf{H} is parallel to each of the three high-symmetry directions. The intersite coupling constant λ is set to $\lambda = 0.03$ K with $z = 4$ neighbors. This leads to the transition temperature $T_c \simeq 0.122$ K at $\mathbf{H} = \mathbf{0}$ and the critical magnetic field along $\mathbf{H} \parallel [001]$: $H_c(001) \simeq 2.46$ T, $H_c(110) \simeq 1.46H_c(001)$, and $H_c(111) \simeq 2.13H_c(001)$ at $T = 0$, which roughly correspond to the experimental data.¹⁰⁾ Anisotropy in the critical field strength is mainly determined by the non-linear Zeeman effect (8). The critical field is largest for $\mathbf{H} \parallel [001]$, then next for $\mathbf{H} \parallel [110]$, and smallest for $\mathbf{H} \parallel [111]$. For $[111]$ direction, the effect (8) vanishes and as discussed before the critical field is determined by the octupole-field coupling as far as the magnetic field is not so strong.

First, let us investigate the case of $\mathbf{H} \parallel [001]$. The phase diagram shows three ordered phases I, II, and III as shown in Fig. 4. The phase-I is a basically antiferro quadrupole state with Q_x type order with small Q_z ferro quadrupole components, and this is discussed in the previous subsection. For finite $|\mathbf{H}|$, there are two stable domains characterized by $(y^2 - z^2)$ and $(z^2 - x^2)$ type sym-

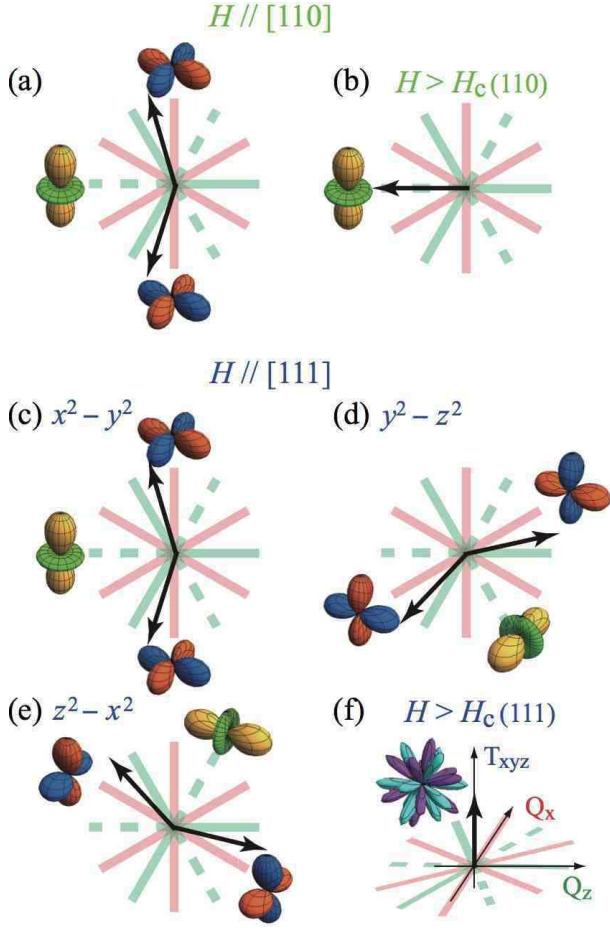


Fig. 6. (Color online) Schematic pictures of the quadrupole orders for $\mathbf{H} \parallel [110]$ and $[111]$. (a) antiferro quadrupole state for $[110]$ direction. (b) high-field state for $[110]$ direction. (c),(d),(e) three domains in antiferro quadrupole state for $[111]$ direction. (f) high-field state for $[111]$ direction. In (f), the third axis represents octupole T_{xyz} .

metries as illustrated in Figs. 5(a) and (b), where two arrows represent order parameters for two sublattices. With increasing the field, the two arrows rotate clockwise in (a), while counterclockwise in (b). This is accompanied by variations in the amplitude of the quadrupole moments $|\mathbf{Q}^A|$ and $|\mathbf{Q}^B|$. This is a natural way to gain the Zeeman energy (8), keeping the (almost) antiparallel configuration. At $|\mathbf{H}| = H_c^{(1)}$, there is a second-order transition to the phase-II, where the two arrows point antiparallel along Q_z direction with different magnitudes as shown in Fig. 5 (c). In the phase-II, the two domains in the phase-I are merged to the same domain, and this is the unique stable domain. Further increasing magnetic field leads to a first-order transition to the phase-III at $|\mathbf{H}| = H_c^{(2)}$, where \mathbf{Q} shows a canted order. The Q_x component exhibit an antiferro order, while $Q_z > 0$ ferro order, as shown in Fig. 5 (d). With increasing magnetic field, the antiferro component decreases, while the ferro component increases. Finally, there ap-

pears a second-order transition at $|\mathbf{H}| = H_c(001)$ from the canted phase-III to the polarized phase IV. In the phase-IV, the order parameter points to Q_z direction on both of A and B sites. The phase-IV is smoothly connected to paramagnetic state above T_c .

Secondly, let us consider the case of $\mathbf{H} \parallel [110]$. In this case, there is only one ordered phase, and the stable domain is also unique. This phase has an antiferro order of $(x^2 - y^2)$ -type quadrupole component accompanied with ferro $Q_z < 0$. This is illustrated in Fig. 6 (a), and this coincides to one of the stable domains in the phase-I when $\mathbf{H} \parallel [100]$ or $[010]$. With increasing field, the Q_z components increase and finally the quadrupole moments align along $-Q_z$ direction at $|\mathbf{H}| = H_c(110)$ through a second-order transition.

Thirdly, for $\mathbf{H} \parallel [111]$, there is also only one ordered phase but three domains are all stable. One domain exhibits negative Q_z as illustrated in Fig. 6 (c), while the other two have positive net Q_z as illustrated in Figs. 6 (d) and (e). Increasing $|\mathbf{H}|$ suppresses Q_z for all the three, and, as discussed in the previous subsection, induces T_{xyz} octupole moment. The transition to the high-field phase at $|\mathbf{H}| = H_c(111)$ is also second order. In the high-field phase, no quadrupole moment exists, while there remains an induced T_{xyz} octupole moments as shown in Fig. 6 (f).

2.7 Physical quantities

In this subsection, we show the details of magnetic field dependence of multipoles \mathbf{Q} , \mathbf{J} , and T_{xyz} . Figure 7 shows these quantities at $T = 0$ and for three directions of the magnetic field. The results for $\mathbf{H} \parallel [001]$ are shown in Fig. 7 (a), where the domain of $(y^2 - z^2)$ -type is chosen for the phase-I. For $\mathbf{H} \parallel [110]$, the stable domain is unique, *i.e.*, $(x^2 - y^2)$ -type, and Fig. 7(b) shows multipole moments along $\mathbf{H} \parallel [110]$. The results for $\mathbf{H} \parallel [111]$ are shown in Fig. 7(c), and the $(x^2 - y^2)$ -type domain is chosen for the ordered phase. Since we have already discussed the variations of \mathbf{Q} in Sect. 2.6, we here discuss a physical origin of induced magnetic moments \mathbf{J} .

To discuss what kinds of multipoles are induced in the presence of both magnetic field and the order parameter \mathbf{Q} , a group theoretical argument is very useful.¹⁶⁾ In Appendix D, a list is shown for the reduction of several products of two irreps. This helps understanding the coupling of \mathbf{J} to \mathbf{H} and \mathbf{Q} , and it is sufficient to notice that \mathbf{Q} transforms as Γ_3 representation, while \mathbf{J} and \mathbf{H} as Γ_4 . The lowest-order local coupling that includes the three quantities is

$$\frac{Q_z - \sqrt{3}Q_x}{2} J_x H_x + \frac{Q_z + \sqrt{3}Q_x}{2} J_y H_y - Q_z J_z H_z. \quad (10)$$

This indicates that antiferromagnetic J_z component is induced by the antiferro Q_z order for $\mathbf{H} \parallel [001]$ as shown in Fig. 7(a), while antiferromagnetic $J_x - J_y$ component is induced for $\mathbf{H} \parallel [110]$ [Fig. 7(b)] and $[111]$ [Fig. 7(c)] by the antiferro Q_x order. Note also that Eq. (10) holds for any Γ_4 operators by replacing \mathbf{J} by them.

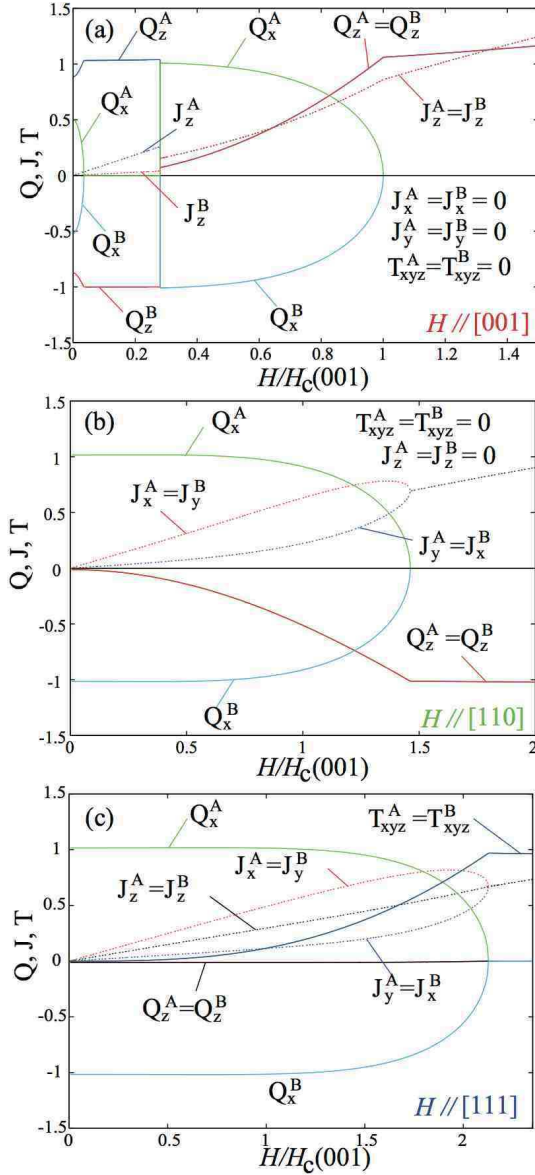


Fig. 7. (Color online) Order parameters vs. magnetic field for (a) $\mathbf{H} \parallel [001]$, (b) $\mathbf{H} \parallel [110]$, and (c) $\mathbf{H} \parallel [111]$.

Similarly, one can construct a coupling between a magnetic Γ_5 operators, *e.g.*, \mathbf{T}^β octupole moment, and \mathbf{H} and \mathbf{Q} ,

$$\frac{\sqrt{3}Q_z + Q_x}{2}T_x^\beta H_x + \frac{-\sqrt{3}Q_z + Q_x}{2}T_y^\beta H_y - Q_x T_z^\beta H_z. \quad (11)$$

Although we do not show the results for Γ_5 operators, \mathbf{T}^β octupole moments are induced as discussed by Shiina *et al.*¹⁶⁾

Now, let us discuss changes in the ground-state wavefunction $|0\rangle_{A,B}$ with \mathbf{H} . With varying the strength of magnetic field, we numerically obtained the mean-field ground state on the *A*- and *B*-sublattices, $|0\rangle_{A,B} = \sum_i \sum_n a_{A,B}(\Gamma_i, n) |\Gamma_i n\rangle_{A,B}$. $w_{A,B}(\Gamma_i n) = |a_{A,B}(\Gamma_i n)|^2$ is the occupation of the basis state n in the Γ_i multiplet

for the paramagnetic state at $\mathbf{H} = \mathbf{0}$ in the ground state, and of course $\sum_{in} w_{A,B}(\Gamma_i n) = 1$.

Figures 8(a)-(e) show the occupation $w_A(\Gamma_i n)$ of the five multiplets as a function of magnetic field strength for three field directions. The states not shown in each panel have occupation negligibly small or exactly zero. The occupation at the *B*-sublattice is the same, $w_B(\Gamma_i n) = w_A(\Gamma_i n)$ except for the case of $\mathbf{H} \parallel [001]$, for which $w_B(\Gamma_i n)$ is shown in Fig. 8(f).

For $\mathbf{H} \parallel [001]$, two stable domains in the phase-I have the same occupations w 's. In the phase-II the wavefunction at the *A*-sublattice is almost pure Γ_{3u} as in the high-field phase, since this is a collinear order. At the *B*-sublattice, $\langle Q_z \rangle \sim -1$ and $\langle Q_x \rangle = 0$, and therefore, the wavefunction is almost a pure Γ_{3v} state. In the phase-III, both Γ_{3u} and Γ_{3v} states have large occupation at each sublattice and their hybridization yields a canted configuration of \mathbf{Q} . With increasing field strength, one of the two states dominates, and correspondingly the ferro Q_z component increases.

Let us check the amplitude of the secondary component and confirm that $\langle Q_z \rangle \neq 0$ at $\mathbf{H} = \mathbf{0}$. Figure 9(a) shows the magnetic-field dependence of ferro Q_z component near $\mathbf{H} = \mathbf{0}$ for $\mathbf{H} \parallel [001]$. As one can clearly see, the ferro component is indeed finite even at $\mathbf{H} = \mathbf{0}$ and the limiting value at $\mathbf{H} = \mathbf{0}$ agrees with that obtained by perturbative expressions (5) and (6).

Temperature dependence of Q_z near T_c exhibits an evidence that the ferro Q_z moment is a secondary order parameter, and induced by Q_x antiferro moment. Figure 9(b) shows the temperature dependence of \mathbf{Q} near T_c . The primary order parameter Q_x shows a typical mean-field criticality, $|Q_x| \propto \sqrt{T_c - T}$, but as for the ferro Q_z component, the temperature dependence is linear, $Q_z \propto -(T_c - T) \propto -Q_x^2$. This fact is consistent with our early analysis based on the third-order anisotropic term in H_{CEF} . As shown in Appendix E, the local Landau free energy has a third-order term. Combining this with the second-order term, the Q_z part of the Landau free energy is given as

$$F_{Q_z} \sim \frac{1}{2\chi} Q_z^2 + \frac{\kappa_3}{\chi^2} Q_x^2 Q_z, \quad (12)$$

where the expression of χ and κ_3 are shown in Appendix E. It is important that Q_x^2 have a static value in the ordered phase below T_c , and therefore, $h_{Q_z} = -\frac{\kappa_3}{\chi^2} Q_x^2$ behaves as a uniform conjugate field of Q_z . The induced moment is then

$$Q_z = \chi h_{Q_z} = -\frac{\kappa_3}{\chi} Q_x^2. \quad (13)$$

This is consistent with the results in Fig. 9(b). This also explains why the induced Q_z moment is ferro Q_z and not antiferro Q_z .

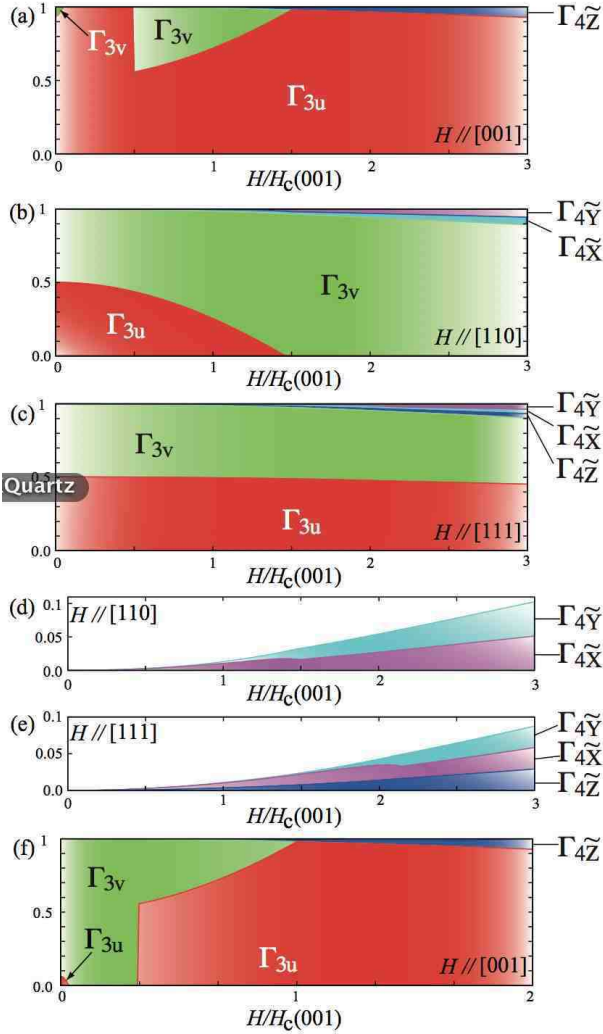


Fig. 8. (Color online) Weights of basis states in the A-site ground state for (a) $\mathbf{H} \parallel [001]$, (b) $\mathbf{H} \parallel [110]$, (c) $\mathbf{H} \parallel [111]$ with the $(x^2 - y^2)$ domain. Zoom up of Γ_4 weights for (d) $\mathbf{H} \parallel [110]$, (e) $\mathbf{H} \parallel [111]$. (f) Weights for B-sublattice for $\mathbf{H} \parallel [001]$.

3. Excitations and Responses

In this section, we will investigate “spin” wave excitations for $T = 0$ and static quadrupole susceptibilities in detail.

3.1 “Spin” wave approximation at zero temperature

In this subsection, we will briefly explain the method of “spin” wave approximation for a general exchange type Hamiltonian.^{29,30} This analysis is equivalent to the equation of motion method with decoupling¹⁷) at $T = 0$, and useful for analyzing excitation spectra. Note, however, that because of the nature of the approximation, the method is valid at low temperatures.

3.1.1 Formulation

We represent the fluctuation beyond the mean-field approximation by using a set of bosons $\{a_{il}\}$ and $\{b_{il}\}$

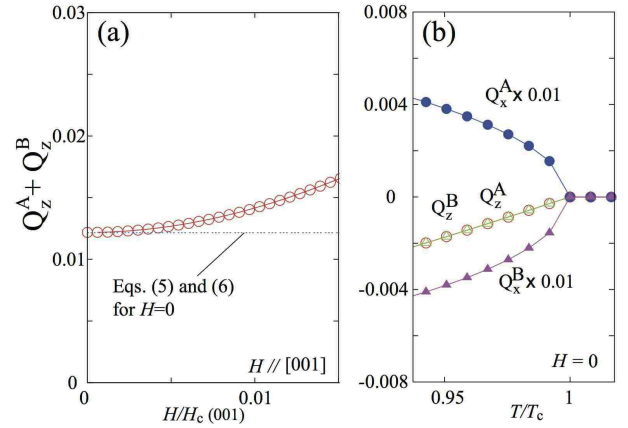


Fig. 9. (Color online) (a) Ferro Q_z moment near $\mathbf{H} = \mathbf{0}$ for $\mathbf{H} \parallel [001]$. The dotted line shows the value calculated by the perturbative analysis. (b) Temperature dependence of quadrupole moments near T_c for $\mathbf{H} = \mathbf{0}$.

and their conjugates. Here, $a_{jl}^\dagger |0\rangle_A$ ($l = 1, \dots, 8$) represents the l th mean-field excited state at the site j in the A-sublattice, while $b_{jl}^\dagger |0\rangle_B$ for B-sublattice, and $|0\rangle_{A,B}$ represents the mean-field ground state at each site. The fluctuation term in our model is

$$H_2 \equiv \lambda \sum_{\langle i,j \rangle} \sum_{\mu=z,x} \left[Q_\mu^A(i) - \langle Q_\mu^A \rangle \right] \left[Q_\mu^B(j) - \langle Q_\mu^B \rangle \right], \quad (14)$$

and in more general cases it is represented as

$$H_2 = \sum_{m,\langle i,j \rangle} \lambda_m \left[O_m^A(i) - \langle O_m^A \rangle \right] \left[O_m^B(j) - \langle O_m^B \rangle \right]. \quad (15)$$

In terms of the introduced boson operators, this reads as

$$H_2 = \sum_{m,l,l',\langle i,j \rangle} \lambda_m \left[(O_m^A)_l a_{il}^\dagger + \text{h.c.} \right] \left[(O_m^B)_{l'} b_{j'l'}^\dagger + \text{h.c.} \right]. \quad (16)$$

Here, $O_m^{A(B)}$ is a general operator at A(B)-sublattice appearing in the Hamiltonian labeled by m and $(O_m^{A(B)})_l$ is the matrix element of $O_m^{A(B)}$ between the ground state and the l th excited state for the A(B)-sublattice. Note that the linear term in the bosons vanishes due to the mean-field condition. Combining on-site excitation energy $E_l^{A(B)}$ for the l th excited state at the A(B)-sublattice, we obtain as a Hamiltonian for the bosons,

$$H_b = \sum_{il} \left(E_l^A a_{il}^\dagger a_{il} + E_l^B b_{il}^\dagger b_{il} \right) + \sum_{m,l,l',\langle i,j \rangle} \lambda_m \left[(O_m^A)_l a_{il}^\dagger + \text{h.c.} \right] \left[(O_m^B)_{l'} b_{j'l'}^\dagger + \text{h.c.} \right]. \quad (17)$$

This Hamiltonian is bilinear in the boson operators and therefore we can diagonalize this by the Bogoliubov transformation to obtain its eigenenergies $\omega_{\mathbf{q}n}$ ($n = 1, \dots, 16$ in our case) with \mathbf{q} being the wavevector.

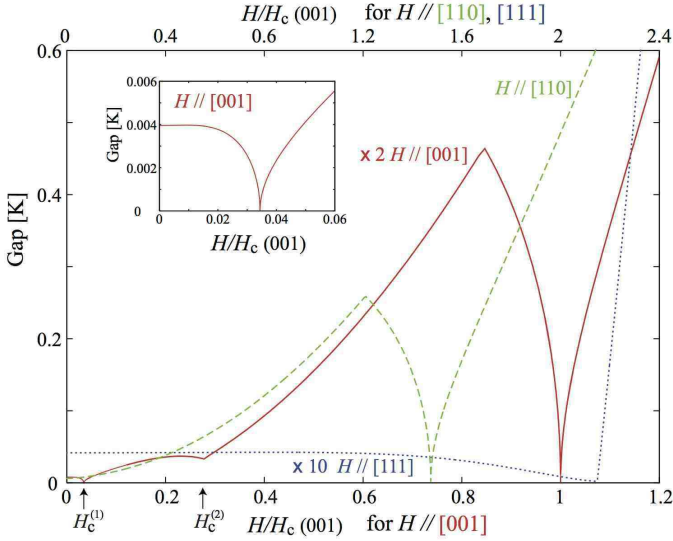


Fig. 10. (Color online) Spin wave excitation gap at $\mathbf{q} = \mathbf{0}$ for $\mathbf{H} \parallel [001]$ (solid line), for $\mathbf{H} \parallel [110]$ (dashed line), and for $\mathbf{H} \parallel [111]$ (dotted line). Beware that the scale of both axes is different depending on field direction. Inset: Zoom up of the low field regime for $\mathbf{H} \parallel [001]$.

3.1.2 Excitation spectrum at zero temperature

Using the boson Hamiltonian introduced above, we now calculate the evolution of excitation energy spectrum with the variation of magnetic-field strength. Diagonalization of H_b is similar to random-phase approximation. However, in contrast to the standard spin-wave theory for magnets, all the local degrees of freedom are taken into account. The inter-site correlations are taken into account only through the channels included in the microscopic Hamiltonian, and they are \mathbf{Q} operators in our case.

Figure 10 shows the lowest excitation gap as a function of magnetic field for the three directions, where $H_c(001)$ is the critical field between the phase-III and the phase-IV for $\mathbf{H} \parallel [001]$. The excitations have an energy minimum at $\mathbf{q} = \mathbf{0}$ for all the parameter regimes. For each \mathbf{H} direction, the excitation becomes gapless at the critical points between the ordered state and the high-field polarized state. This is very similar to the case in transverse-field Ising systems. For $\mathbf{H} \parallel [001]$, there is an additional gapless point at $|\mathbf{H}| = H_c^{(1)}$ between the phase-I and the phase-II. At the first-order transition point $|\mathbf{H}| = H_c^{(2)}$ between the phase-II and the phase-III, the magnetic field dependence of the gap exhibits a small jump (not visible in the scale in Fig. 10). One can see kinks near $H/H_c(001) \sim 0.8$ for $\mathbf{H} \parallel [001]$ and $H/H_c(001) \sim 1.2$ for $\mathbf{H} \parallel [110]$. These are not due to any phase transitions but due to level crossing between different excited states.

Let us note that the scaling of the gap near the critical fields. For $\mathbf{H} \parallel [001]$ and $[110]$, the gap varies as $\propto |\delta H|^{1/2}$, where δH is the deviation from the critical field H_c for each magnetic-field direction: $\delta H \equiv H - H_c$.

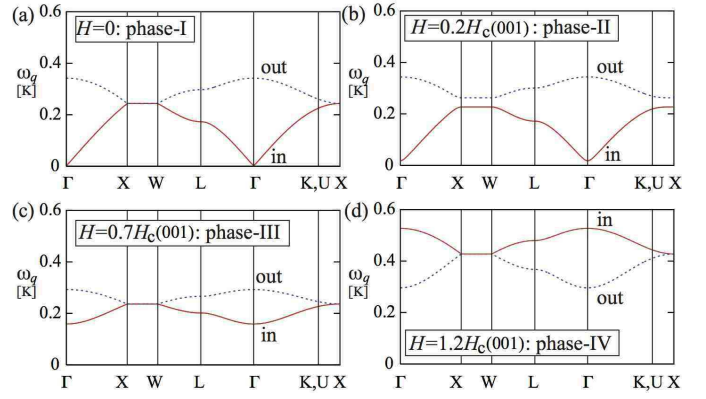


Fig. 11. (Color online) Excitation spectra for $\mathbf{H} \parallel [001]$. Full-red (dotted-blue) lines represent “in” (“out”) mode. See the text for the definition of the modes. (a) phase-I for $\mathbf{H} = \mathbf{0}$, (b) phase-II for $|\mathbf{H}| = 0.2H_c(001)$, (c) phase-III for $|\mathbf{H}| = 0.7H_c(001)$, and (d) phase-IV for $|\mathbf{H}| = 1.2H_c(001)$. Notations: $\Gamma : \mathbf{q} = (0, 0, 0)$, $X : (2\pi, 0, 0)$, $W : (\pi, 0, 2\pi)$, $L : (\pi, \pi, \pi)$, $K : (\frac{3\pi}{2}, \frac{3\pi}{2}, 0)$, and $U : (\frac{\pi}{2}, 2\pi, \frac{\pi}{2})$, where the lattice constant is set to unity.

Interestingly, the gap for $\mathbf{H} \parallel [111]$ varies as $|\delta H|^{3/2}$ for $H < H_c(111)$ and as $|\delta H|$ for $H > H_c(111)$. This leads to unusual divergence in susceptibilities near the critical point for $\mathbf{H} \parallel [111]$. We will discuss this in more detail in Sects. 3.2.1 and 3.2.2.

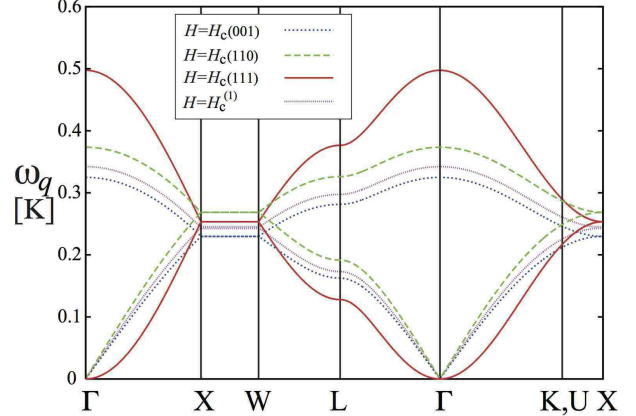


Fig. 12. (Color online) Excitation spectra at critical fields: $|\mathbf{H}| = H_c(001)$, $H_c(111)$, $H_c(110)$ and $H_c^{(1)}$ for $\mathbf{H} \parallel [001]$.

The dependence of the excitation spectra on wavevector \mathbf{q} is shown in Fig. 11 for $\mathbf{H} \parallel [001]$. For other directions, we obtain similar results, and we do not show them here. Since the energy scale of the interaction λ is much smaller than local energies in H_{CEF} , the high energy modes are similar to local CEF excitations and their \mathbf{q} -dependence is very small. Therefore, we show here only the lowest two modes, which consist mainly of the non-Kramers Γ_3 doublet. It is noted that the number of the modes does not change in all the phases, since only $\mathbf{q} = \mathbf{0}$

orders are considered in this paper.

First, we discuss the nature of these two lowest-energy modes. They are rotation of $\mathbf{Q}^{A,B}$ in the two-dimensional \mathbf{Q} -space from the ground-state configuration in each phase. There are basically two types of rotations. One is an in-phase rotation of \mathbf{Q}^A and \mathbf{Q}^B ; that is, the two quadrupole moments rotate in the same direction. The other is an out-phase rotation; the two rotate in an opposite direction. We label them by “in” and “out” in Fig. 11. Note that in the phase-III a level crossing occurs between these two excitations as shown in Fig. 10. This means that “in” and “out” are interchanged for the higher field part of the phase-III. Figure 11 (c) shows the spectra in the lower field part.

To understand the nature of each of these modes, it is easiest to study the high-field phase-IV. In the high-field phase, the lowest-energy excitation is the “out” mode and thus has a finite matrix element of staggered Q_x with the ground state. Since the system starts to exhibit the Q_x antiferro quadrupole order as the magnetic field decreases, this is natural and it is this softening that leads to the phase transition. For other phases, similar arguments are also possible.

Secondly, we note that the flat band in the excitation spectrum along X-W direction has the same energy as the lowest excited level of an isolated single site calculated by the mean-field theory. This is because the form factor of the diamond lattice structure vanishes there. One can see that the two modes in Fig. 11 are degenerate along X-W except for (b). This is related to the symmetry between A - and B -sublattices for $|\mathbf{H}| = 0$ and $H_c^{(2)} < |\mathbf{H}|$, while there is no such symmetry for $0 < |\mathbf{H}| < H_c^{(2)}$, since $|\mathbf{Q}^A| \neq |\mathbf{Q}^B|$.

Finally, we show the excitation spectra at the critical fields in Fig. 12. At or near the continuous transition for $\mathbf{H} \parallel [001]$ and $[110]$, the energy dispersion is $|\mathbf{q}|$ -linear around the Γ point, which also indicates that the system becomes critical. At the critical field for $\mathbf{H} \parallel [111]$, however, the dispersion is $|\mathbf{q}|^2$ and this is due to the absence of induced quadrupole moment in this field direction. This is qualitatively understood by considering an effective pseudospin-1/2 XY model with a field perpendicular to the XY plane. This corresponds to the fact that the inter-site interactions are only about the quadrupoles, while the magnetic field couples with the octupole when $\mathbf{H} \parallel [111]$. Within the spin-wave approximation, anomalous terms $a_i^\dagger b_j^\dagger$ and $a_i b_j$ vanish and only hopping terms $a_i^\dagger b_j$ and $b_j^\dagger a_i$ remain in Eq. (17). This is the same for spin waves in isotropic ferromagnets and there the dispersion is $|\mathbf{q}|^2$.

3.2 Quadrupole susceptibilities

In this subsection, we study the quadrupole susceptibilities. We first show the numerical results of the quadrupole susceptibilities as a function of magnetic field for three symmetric directions in Sect. 3.2.1. As we will

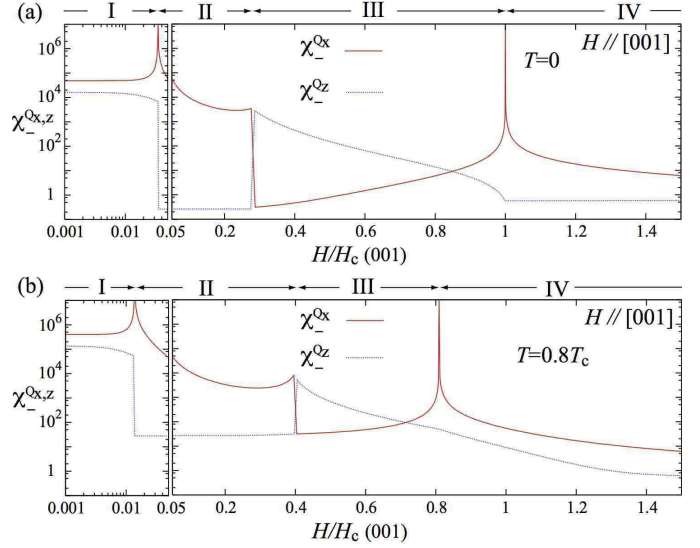


Fig. 13. (Color online) Quadrupole susceptibility $\chi_{-}^{Qx, Qz}$ vs. magnetic field $\mathbf{H} \parallel [001]$. (a) $T = 0$ and (b) $T = 0.8T_c$ ($\mathbf{H} = \mathbf{0}$).

show, unusual critical behaviors appear for $\mathbf{H} \parallel [111]$, and to clarify them, we analyze the nature of the unusual criticality in Sect. 3.2.2.

3.2.1 Numerical results

Let us first define two components of the susceptibilities with respect to the sublattice indices. Because of A and B sublattices, the quadrupole susceptibility is a 2×2 matrix, and we consider two parity-conserving responses that are also diagonal in \mathbf{Q} -space. Just for notational convenience, we denote them in terms of χ_{\pm}^{\pm} in Eq. (F.7) as $\chi_{\pm}^{Q\mu} = (\chi_{\pm}^{\pm})_{\mu\mu}$, where $\mu = z$ or x . In the following, we will study the behavior of these quadrupole susceptibilities upon changing magnetic field strength for three special field directions.

- $\mathbf{H} \parallel [001]$:

Figure 13 shows the staggered part of the static quadrupole susceptibility, $\chi_{-}^{Q\mu}$ as a function of magnetic field applied along $[001]$ direction. Note that the staggered part here refers to the component with $\mathbf{q} = \mathbf{0}$ that has an odd parity for exchange of A and B sites, instead of finite- \mathbf{q} component. The most prominent feature is divergence at two phase boundaries. The divergence at higher field takes place at the transition between phases III and IV, while the divergence at lower field concurs with the transition between phases I and II at $H_c^{(1)} \sim 0.03H_c(001)$. The staggered order parameter, $\langle Q_x^A \rangle - \langle Q_x^B \rangle$, is zero in the phases II and IV, and this continuously emerges upon moving into the phases I and III. The divergence of χ_{-}^{Qx} is a consequence of this continuous phase transition. Another prominent feature is a large jump at $H_c^{(2)} \sim 0.3H_c(001)$. This is due to the first-order phase transition between the phases II and III. Just

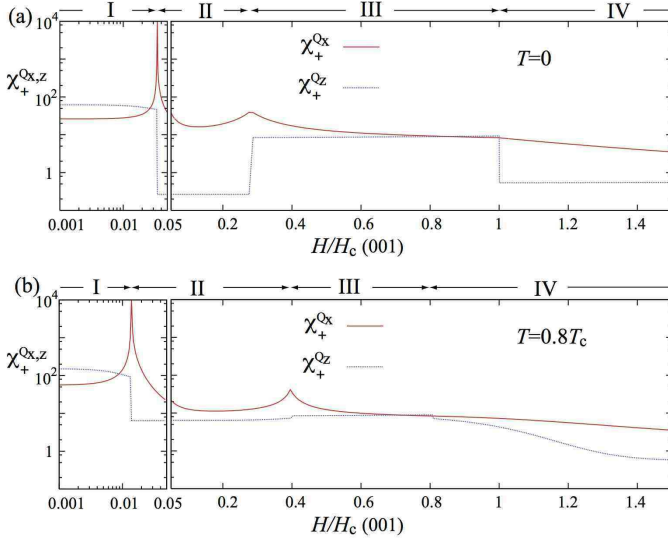


Fig. 14. (Color online) Quadrupole susceptibility $\chi_+^{Qx, Qz}$ vs. magnetic field $\mathbf{H} \parallel [001]$ (a) $T = 0$ and (b) $T = 0.8T_c$ ($\mathbf{H} = \mathbf{0}$).

above $H_z^{(2)}$ in the phase III, the quadrupole moments are aligned almost parallel to Q_x direction, and their size is large $|\langle Q_x^{A,B} \rangle| \sim 1$, as shown in Fig. 7(a). Therefore, their fluctuations are suppressed and this leads to a reduction of χ_-^{Qx} . The quadrupole order is completely different in the phase II, which is below $H_c^{(2)}$. The quadrupole moments are aligned to $\pm Q_z$ direction. Therefore, their transverse fluctuations contribute to χ_-^{Qx} , and its value is quite large.

Singularity is found also in the uniform part of the static susceptibility, χ_+^{Qx} , as shown in Fig. 14, although this singularity is weaker than that in the staggered part χ_-^{Qx} . At the transition point between the phases IV and III, the uniform susceptibility does not diverge but shows a kink. See the (red) line near $H \sim H_c(001)$. The absence of divergence comes from the fact that the corresponding static quantity $\langle Q_x^A \rangle + \langle Q_x^B \rangle$ is not an order parameter in either of the phases III and IV. However, this quantity couples to the order parameter and this leads to a kink singularity in its field dependence. This is similar to the singularity in uniform susceptibility of antiferromagnets at the Neel temperature. This kink behavior is enhanced with lowering temperature. The transition between the phases III and II is first order, and χ_+^{Qx} shows a small jump there. The transition between the phases II and I is special, and the uniform susceptibility also diverges. This is because in the phase I $|\langle Q_x^A \rangle| \neq |\langle Q_x^B \rangle|$, while both vanish in the phase II. Therefore, not only the staggered part but also the uniform part have fluctuations that diverge with approaching the transition point, which leads to $\chi_{\pm}^{Qx} \rightarrow \infty$. As for χ_+^{Qz} , it is suppressed in collinear phases with $\langle Q_x \rangle = 0$ such as in the phases II and IV, while enhanced in the phases I and III. This is natural, since longitudinal fluctuations are expected weaker than

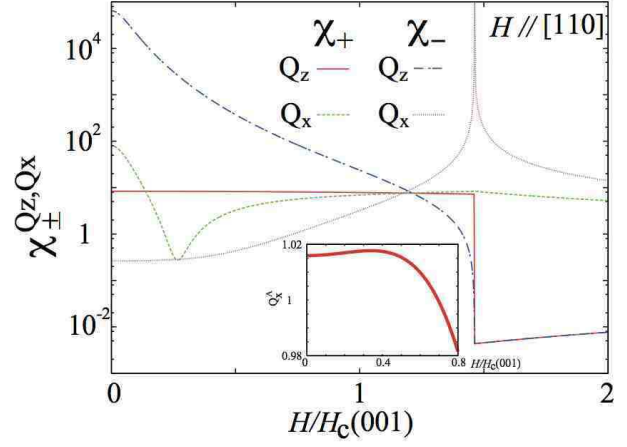


Fig. 15. (Color online) Quadrupole susceptibility vs. magnetic field for $\mathbf{H} \parallel [110]$. Inset: $\langle Q_x^A \rangle = -\langle Q_x^B \rangle$ at low fields.

transverse ones.

- $\mathbf{H} \parallel [110]$:

Figure 15 shows $\chi_{\pm}^{Qz, x}$ at $T = 0$ and for $\mathbf{H} \parallel [110]$. In addition to the divergence in χ_-^{Qx} at the critical field, one can see a dip in χ_+^{Qx} at low fields. Indeed, $\langle Q_x \rangle$ shows a non-monotonic behavior in the low-field regime as shown in the inset of Fig. 15, and more directly, the weight of the lowest-energy eigen mode related to $Q_x^A + Q_x^B$ vanishes at the magnetic field where χ_+^{Qx} is a minimum, while the change in eigenenergy is monotonic as shown in Fig. 10.

- $\mathbf{H} \parallel [111]$:

For $\mathbf{H} \parallel [111]$, there is only one transition and the susceptibilities show unusual magnetic-field dependence near the critical field. To be specific, we choose the $(x^2 - y^2)$ domain in the ordered phase [see Fig. 6 (c)]. Figure 16 shows that not only the staggered components $\chi_-^{Qz, Qx}$ but also the uniform component χ_+^{Qx} diverge at the critical field $H_c(111)$. It is interesting to note that χ_+^{Qx} diverges *only* in the ordered phase. The singularities of static $\chi_{\pm}^{Qz, Qx}$ are summarized in Table I. Note that the strong singularity for $\chi_-^{Qz} \propto |\delta H|^{-2}$ in the ordered phase makes a striking contrast to the conventional mean-field divergence $\sim |\delta H|^{-1}$ in the other field directions. We will investigate the origin for these unusual behaviors in the next subsection.

Table I. Singularity of the quadrupolar susceptibilities near the critical field $H_c(111)$ for $\mathbf{H} \parallel [111]$ and those near the critical temperature T_c at $\mathbf{H} = \mathbf{0}$. Here, $\delta H = H - H_c$ and $\delta T = T - T_c$.

	$\mathbf{H} \parallel [111]$		$\mathbf{H} = \mathbf{0}$	
	$H < H_c$	$H > H_c$	$T < T_c$	$T > T_c$
χ_-^{Qz}	$ \delta H ^{-2}$	δH^{-1}	$ \delta T ^{-2}$	δT^{-1}
χ_-^{Qx}	$ \delta H ^{-1}$	δH^{-1}	$ \delta T ^{-1}$	δT^{-1}
χ_+^{Qz}	$\sim \text{const.}$	$\text{const.} - \delta H$	$\sim \text{const.}$	$\text{const.} - \delta T$
χ_+^{Qx}	$ \delta H ^{-1}$	$\text{const.} - \delta H$	$ \delta T ^{-1}$	$\text{const.} - \delta T$

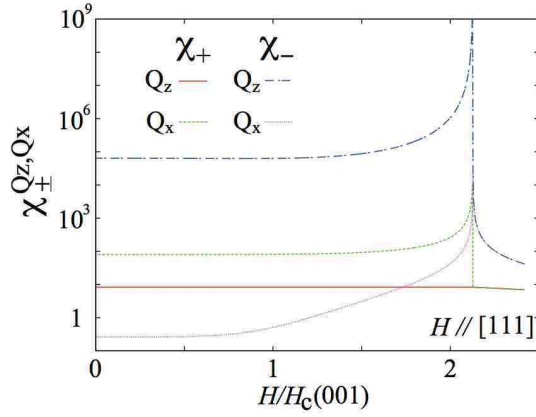


Fig. 16. (Color online) Quadrupole susceptibility vs. magnetic field for $\mathbf{H} \parallel [111]$.

3.2.2 Analysis on unusual divergences in susceptibilities

In this subsection, we show that the A - B sublattice mean-field approximation can explain those discovered unusual divergences in χ 's if the Z_3 anisotropy in \mathbf{Q} -space is correctly taken into account. Recall that this occurs for increasing magnetic field $\mathbf{H} \parallel [111]$. As will be discussed, this also happens near the transition temperature at $\mathbf{H} = \mathbf{0}$.

In Appendix F, we show the formula of the uniform and staggered quadrupole susceptibilities χ^\pm in terms of the local susceptibility $\chi_{\text{loc}}^{A,B}$. In this subsection, we will analyze $\chi_{\text{loc}}^{A,B}$ calculated by the Landau theory developed in Appendix G, and show that the susceptibilities indeed exhibit unusual singularities as discussed in the previous subsection.

First, let us calculate the local susceptibility from single-site free energy F_{AFQ}^s valid for $\mathbf{H} \parallel [111]$ or $\mathbf{H} = \mathbf{0}$:

$$F_{\text{AFQ}}^s = \frac{a}{2} |\mathbf{Q}^s|^2 - \frac{\gamma}{3} [Q_z^s(Q_z^{s2} - 3Q_x^{s2})] + \frac{b}{4} |\mathbf{Q}^s|^4, \quad (18)$$

where $s = A$ or B is the site index. We consider a domain in the ordered phase where $\langle Q_x^A \rangle = -\langle Q_x^B \rangle = q_s$ and $\langle Q_z^{A,B} \rangle = -q_u$. Here, q_s and q_u are given by Eqs. (G.4) and (G.6). The free energy F_{AFQ}^s is expanded up to the second order in the fluctuation $\delta \mathbf{Q}^s = \mathbf{Q}^s - \langle \mathbf{Q}^s \rangle$ and we obtain

$$F_{\text{AFQ}}^s = F_{\text{AFQ}}^{s0} + \frac{1}{2} \delta \mathbf{Q}^s \cdot \left(\chi_{\text{loc}}^s \right)^{-1} \cdot \delta \mathbf{Q}^s. \quad (19)$$

Here, F_{AFQ}^{s0} is the free energy at the stationary point. In this domain, χ_{loc}^B is identical to χ_{loc}^A except the sign of the off-diagonal elements. In terms of the parameters in Appendix G, we obtain

$$\left(\chi_{\text{loc}}^A \right)_{\mu\mu} \sim \frac{1}{g} + c_\mu^{(1)} \delta h + c_\mu^{(2)} \delta h^2, \quad (20)$$

$$\left(\chi_{\text{loc}}^A \right)_{zx} \sim t_1 \delta h^{1/2} + t_2 \delta h^{3/2}, \quad (21)$$

where g is the effective intersite quadrupole coupling and

$\delta h = g - a$ is the control parameter representing the distance from the critical point, and

$$c_z^{(1)} = \frac{2\gamma^2/g}{g^2 \tilde{b}}, \quad c_x^{(1)} = -\frac{2(b - 2\gamma^2/g)}{g^2 \tilde{b}}, \quad t_1 = \frac{2\gamma}{g^2 \sqrt{\tilde{b}}}, \quad (22)$$

with $\tilde{b} = b - \gamma^2/g$. Pay attention to the relation

$$c_z^{(1)} = \frac{1}{2} g t_1^2, \quad (23)$$

and this is the *key* to the unusual singularities. This results in a cancellation of the δh^1 -order term in the calculation of $\det(1 - g^2 \chi_{\text{loc}}^A \chi_{\text{loc}}^B)$ and enhances singularities in various channels. Calculating the higher-order correction coefficients $c_z^{(2)}$, $c_x^{(2)}$, and t_2 , we obtain the leading singularities as

$$\chi_-^{Qz} \sim \frac{4\tilde{b}^2 g^3}{3\gamma^2(3\tilde{b}g + 2\gamma^2)} \delta h^{-2}, \quad (24)$$

$$\chi_-^{Qx} \sim \delta h^{-1}, \quad (25)$$

$$\chi_+^{Qz} \sim \frac{b}{\tilde{b}g}, \quad (26)$$

$$\chi_+^{Qx} \sim \frac{4\tilde{b}g}{3(3\tilde{b}g + 2\gamma^2)} \delta h^{-1}. \quad (27)$$

These are exactly what we have obtained in Sect. 3.2.1.

Note that the change of control parameter $g - a$ can be also driven by temperature, *i.e.*, $\delta h = g - a(H, T)$. Therefore, the same singularities appears at $|\mathbf{H}| = H_c(111)$ for $\mathbf{H} \parallel [111]$ and at the critical temperature for $\mathbf{H} = \mathbf{0}$ by regarding $\delta h \propto \delta H$ or $\propto \delta T$ as shown in Table I. Indeed, we have checked this by microscopic mean-field calculations as shown in Fig. 17. The result of χ_-^{Qz} and χ_+^{Qx} are very unique and interesting. When the anisotropy is decreased $\gamma \rightarrow 0$, the amplitude of the divergence of χ_-^{Qz} itself diverges as $1/\gamma^2$. In isotropic systems, we know that the transverse susceptibility should be infinite in the whole region of its ordered phase as a consequence of gapless Goldstone mode. The behavior found here is in this sense consistent.

4. Discussions

In this section, we will discuss several topics relevant to Pr-based 1-2-20 compounds based on the results in this paper.

4.1 Ferro quadrupole order

In this paper, we have studied antiferro quadrupole orders, which appear in several Pr 1-2-20 compounds. As for PrTi₂Al₂₀, it is suggested that the ordered state is ferro quadrupole.^{6, 14, 28} We briefly discuss below properties of Γ_3 ferro quadrupole order.

Also for the ferro quadrupole case, the discussion on $O_2^2(Q_x)$ order in Sect. 2.2 holds and it is generally accompanied by a finite $O_2^0(Q_z)$ component. Neutron scattering experiment suggests that the order is ferro O_2^0 ,¹⁴ and,

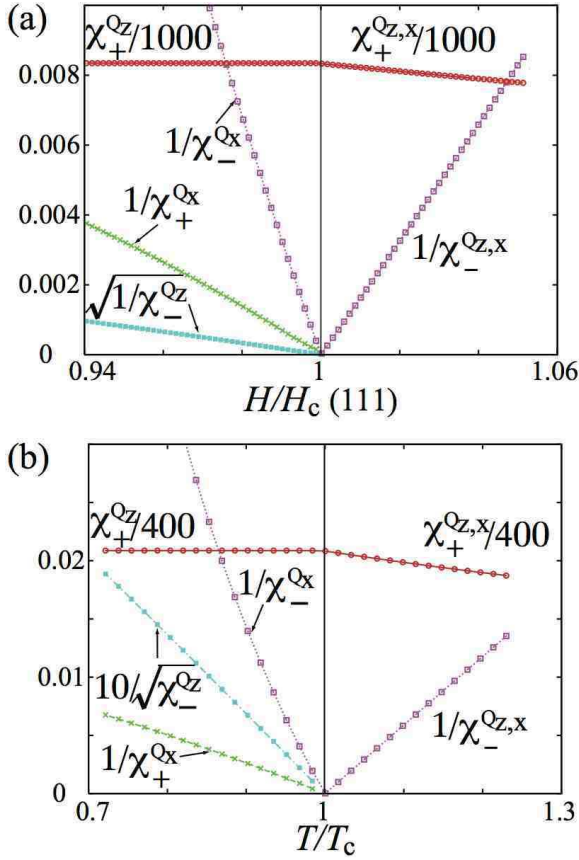


Fig. 17. (Color online) Quadrupole susceptibility near critical points. (a) $\mathbf{H} \parallel [111]$ at $T = 0$. (b) $\mathbf{H} = 0$.

in this case, there is no induced O_2^2 moment from our discussions in Sect. 2.2.

An important difference from the antiferro quadrupole order is the order of the transition. It is generally first-order as predicted by the Landau theory. The Landau free energy F_{FQ} is given as

$$F_{\text{FQ}} \sim \frac{1}{2}a|\mathbf{Q}|^2 + \frac{1}{3}\gamma Q_z(Q_z^2 - 3Q_x^2) + \frac{1}{4}b|\mathbf{Q}|^4. \quad (28)$$

Here, a , b , and γ are constants and \mathbf{Q} is the uniform quadrupole moment. Note that for antiferro quadrupole case \mathbf{Q}_{AF} , the third-order term including three \mathbf{Q}_{AF} 's is not present due to the inversion symmetry ($A \leftrightarrow B$). The possibility of the first-order transition for the antiferro case is discussed in Appendix G.

The third-order anisotropy γ is generally finite unless microscopic parameters are finely tuned. Thus, the transition should be first-order in general cases.³¹⁾ The order of the transition can be controlled by, for example, applying magnetic field. Since the quadrupole couples with magnetic field through Eq. (8), there appears a linear term in F_{FQ} , leading to a finite moment $\langle \mathbf{Q} \rangle$ induced. Then, the situation is similar to the classical liquid-gas transition and it is possible to tune the system to a second-order transition point and also crossover regime

by varying the magnetic field and temperature.

Recently, Matsubayashi et al., observed that the superconducting transition temperature for $\text{PrTi}_2\text{Al}_{20}$ is enhanced near the region where the ferro quadrupole order disappears under pressure.⁸⁾ We expect that this is due to critical or strongly enhanced quadrupole fluctuations of orbital degrees of freedom. However, if the order is ferro quadrupole, the transition is generally first order as discussed before. Then, fluctuations are not so particularly enhanced near the transition, unless the transition is very weak first order. For quantitative comparison with experimental data, we need more elaborate calculations with parameter tuning, which is left for a future study.

4.2 Softening in elastic constants in $\text{PrIr}_2\text{Zn}_{20}$

Uniform quadrupole susceptibility is measured indirectly by ultrasonic experiments through the coupling of elastic constant and quadrupole susceptibility.³²⁾ In systems with T_d symmetry, one measures the elastic constants $c_{11} - c_{12}$ and the c_{44} to detect Γ_3 and Γ_5 quadrupoles, respectively. $c_{11} - c_{12}$ gives information about uniform quadrupole susceptibilities in Γ_3 sector: $\chi_+^{Qz, Qx}$, while c_{44} does about Γ_5 quadrupoles, which are due to the excited states in the 1-2-20 compounds. In $\text{PrIr}_2\text{Zn}_{20}$, the elastic constants exhibit unusual behaviors as a function of magnetic field and temperature.¹⁰⁾ In this subsection, we discuss two aspects of them.

For $\mathbf{H} = 0$, the elastic constants exhibit softening near the transition temperature both in the $c_{11} - c_{12}$ and the c_{44} modes. Since the CEF ground state is the Γ_3 doublet, the softening in $c_{11} - c_{12}$ is due to its degeneracy, which leads to $\sim -1/T$ at low temperature for $T > T_c$ (note that this does not diverge at T_c , since the transition occurs in the antiferro quadrupole sector). However, that in c_{44} mode cannot be explained by a simple picture, since the excited states are in high energy above ~ 30 K and there is no Γ_5 in the direct product $\Gamma_3 \otimes \Gamma_3$. See, Appendix D. As a source of the softening in the c_{44} mode, the effects of mode-mode coupling might be important in this compound. For $c_{11} - c_{12}$ mode, our result in Sects. 3.2.1 and 3.2.2 demonstrates that one of χ_+^{Qx} and χ_+^{Qz} susceptibilities depending on its domain diverges in the ordered phase toward the critical temperature and this is consistent with the experiment.

Under magnetic fields, the elastic constants also exhibit softening as a function of the magnetic field near the high-field critical point.¹⁰⁾ When the magnetic field is applied in $[100]$ direction, c_{11} (a part of Γ_3 mode) shows strong softening as a function of magnetic field and also of temperature at 5 T. In addition, there are two anomalies below 5 T, suggesting the existence of multiple phases under the magnetic field.

For other directions, the elastic constant in Γ_3 mode also shows softening. Our mean-field result is consistent with those for $\mathbf{H} \parallel [111]$ in the ordered phase, while in other cases the origin of the softening is beyond the

mean-field approximation. In addition, there are several anomalies for $\mathbf{H} \parallel [110]$ and $[111]$.^{10,11)} Further experimental works will clarify the nature of the anomalies and the whole T - H phase diagram.

It is noted that the number of phases for $\mathbf{H} \parallel [001]$ suggested in these experiments is consistent with the present results, which is also consistent with the early analysis by Onimaru.²⁴⁾ Thus, one can expect that the strong softening around 5 T is related to the quantum critical point of antiferro quadrupole order between the phase-III and the phase-IV. This is a promising scenario and we need to carry out more elaborate calculations beyond the mean-field approximation, since the diverging susceptibility is not the uniform quadrupole susceptibility but the antiferro quadrupole one at $H_c(001)$ for $\mathbf{H} \parallel [001]$.

It is also instructive to point out that the uniform quadrupole susceptibility diverges when the sizes of corresponding quadrupole moments at two sublattices are different and they vanish at the transition. This situation is realized between the phase-I and the phase-II. The origin of the enhancement in the uniform quadrupole susceptibility near the transition between the phase-II and the phase-III is also related to this.

4.3 Thermo-electric power

Recently, Izawa *et al.*, observed strong enhancement in thermo-electric power S in $\text{PrIr}_2\text{Zn}_{20}$ as a function of temperature under high magnetic fields.³³⁾ The peak position coincides with the peak position of specific heat.³⁴⁾ With decreasing magnetic field, the peak position shifts to a lower temperature and seems to vanish at the critical field ~ 5 T. This suggests that the peak position is related to some energy scale of dynamics. A candidate of this energy scale is the “spin”-wave gap at $\mathbf{q} = \mathbf{0}$ as discussed in Sect. 3.1.2. This explains the \mathbf{H} dependence of specific heat peak position and the fact that the peak temperature vanishes at the critical field. Since in Kondo systems, a peak appears around the Kondo temperature,^{35,36)} to clarify which energy scale determines the peak in S , one needs to carry out more elaborate calculations for non-magnetic Γ_3 systems including both the on-site Kondo screening and inter-site correlations.

4.4 Other intersite interactions

In the present study, we have studied the canonical and minimal model with only quadrupole coupling, and have not included magnetic interactions or other non-magnetic ones. To quantitatively reproduce the phase diagram observed in the experiments, it is necessary to include other interaction, *e.g.*, magnetic dipole interaction and also to carry out calculations beyond the mean-field approximation. Here, we examine the types of possible interactions based on symmetry arguments. See, details in Appendix H.

In Pr-based 1-2-20 compounds, Pr ions form a diamond lattice structure. In the following, we list some of the nearest-neighbor interactions possible in this case.

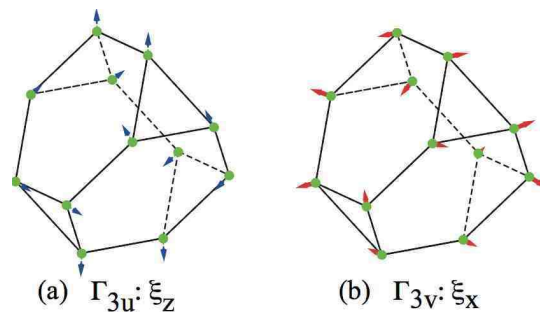


Fig. 18. (Color online) An example of local Γ_3 phonon mode of the cage X_{12} ($X=\text{Zn}$, or Al). Arrows show directions of displacement. (a) $\Gamma_{3u} : \xi_z$ and (b) $\Gamma_{3v} : \xi_x$.

First, as for the quadrupole-quadrupole interactions, only one type is possible, and this is the one used in the present paper.

Second, as for the dipole-dipole interactions, there are two types allowed and they are given as

$$g_1 \mathbf{J}(i) \cdot \mathbf{J}(j) + g_2 [\hat{r}_{ji} \cdot \mathbf{J}(i)] [\hat{r}_{ji} \cdot \mathbf{J}(j)]. \quad (29)$$

Here, i and j are nearest neighbors on different sublattices and $\hat{r}_{ji} = \mathbf{r}_{ji}/|\mathbf{r}_{ji}|$ is the unit vector from i to j . The first term is isotropic in both of \mathbf{J} space and real space, while the second is anisotropic in both spaces.

Thirdly, as for the octupole moments, in addition to trivial $T_{xyz}(i)T_{xyz}(j)$ type interaction, the T_{xyz} octupole can couple with dipole moments as

$$g_3 \left\{ T_{xyz}(i) [\hat{r}_{ji} \cdot \mathbf{J}(j)] + T_{xyz}(j) [\hat{r}_{ji} \cdot \mathbf{J}(i)] \right\}. \quad (30)$$

There are many others, but we stop here and leave them in future publications.

It is noted that the interactions listed above include directional ones, *i.e.*, those including \hat{r}_{ji} . These anisotropic interactions are in general important in the f-electron systems and might lead to different ground states from the simple Γ_3 - Γ_3 model. In order to determine these coupling constants, inelastic neutron scattering is powerful and one can compare the spin-wave dispersions between the experiments and the theory.

4.5 Interactions with phonons

Quadrupole moments are located at the center of a cage and they couple with local phonons of the cage atoms. In particular for the Γ_3 -type mode of displacements denoted as $\xi(i) = [\xi_z(i), \xi_x(i)]$ (see Fig. 18), this couples linearly with the quadrupole at the center as $\mathbf{Q}(i) \cdot \xi(i)$.

It would be more interesting to consider 16c site displacements in the 1-2-20 compounds. The 16c site (Zn or Al) is located at the middle of a nearest-neighbor Pr-Pr bond. The first-principle calculations³⁷⁾ for La compounds suggest that its atom oscillation is highly anharmonic and anisotropic with the hard axis along the bond direction. We denote the displacement of this oscillation

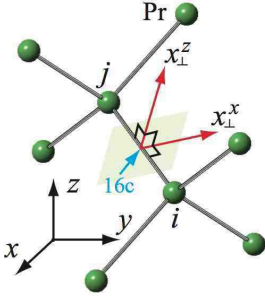


Fig. 19. (Color online) Transverse displacement $\mathbf{x}_\perp(ij)$ at the 16c site located at the bond center.

at the center of the ij bond as $\mathbf{x}_{ij} \equiv (x_{ij}, y_{ij}, z_{ij})$. It can couple with the quadrupole pair as

$$g_4[\mathbf{Q}(i) - \mathbf{Q}(j)] \cdot \mathbf{x}_\perp(ij), \quad (31)$$

where $\mathbf{x}_\perp(ij) = [x_\perp^z(ij), x_\perp^x(ij)] \equiv [(2r_{ji}^z z_{ij} - r_{ji}^x x_{ij} - r_{ji}^y y_{ij})/\sqrt{6}, (r_{ji}^x x_{ij} - r_{ji}^y y_{ij})/\sqrt{2}]$ is the transverse component perpendicular to the bond direction as shown in Fig. 19. This evidently indicates that the presence of antiferro quadrupole order induces a static displacement $\mathbf{x}_\perp(ij)$ in the plane perpendicular to the bond direction. The direction in the plane is determined by the type of the quadrupole order. This also causes inversion symmetry breaking, since the 16c site is an inversion center.

Concerning the displacement $\mathbf{x}_\perp(ij)$, it is also interesting that this induces the Dzyaloshinskii-Moriya interactions. This is given by

$$\mathbf{D}_{ij} \cdot [\mathbf{J}(i) \times \mathbf{J}(j)], \quad (32)$$

where the Dzyaloshinskii-Moriya vector is $\mathbf{D}_{ij} \propto \mathbf{x}_\perp(ij) \times \hat{r}_{ji}$ in the lowest order in the displacement. This term favors incommensurate magnetic ordered states in general. There are many other interactions induced by $\mathbf{x}_\perp(ij)$, but we leave them for future studies.

5. Summary

We have investigated antiferro quadrupole orders in the systems where local ground state is a non-Kramers Γ_3 doublet. We have considered this system on a diamond lattice to discuss orders in Pr-based 1-2-20 compounds, but most of the results in the present study also hold for general bipartite lattices with cubic symmetry. We have analyzed a minimal model for antiferro quadrupole orders based on the mean-field approximation and the quantum fluctuations are also analyzed via “spin”-wave calculations.

We have clarified how anisotropy in crystalline-electric-field potential affects the quadrupole order parameter \mathbf{Q} , and thus, the phase diagrams under magnetic fields. The third-order nontrivial coupling in the quadrupoles is essential to explain it. One important consequence is that there is no pure O_2^2 antiferro quadrupole order without fine tuning of control parameters and the

O_2^2 antiferro quadrupole order is accompanied by ferro O_2^0 quadrupole moments.

The magnetic field-temperature phase diagram shows varieties of phases. They are explained by competitions between the nonlinear Zeeman coupling (8) and antiferro quadrupole inter-site coupling λ . For $\mathbf{H} \parallel [001]$, three ordered phases appear apart from the high-field phase where the quadrupole moments align as determined by the nonlinear Zeeman coupling. The first is a low-field O_2^2 antiferro quadrupole phase. The second is a collinear O_2^0 antiferro quadrupole state. The third is a canted phase. For $\mathbf{H} \parallel [110]$ and $[111]$, there is only one ordered phase and it is a canted state.

To examine excitation dynamics of quadrupole moments, we have analyzed excitation spectra by using “spin”-wave approximation. At the phase boundaries of the second-order transition, there appears a critical mode with linear energy dispersion $\omega \sim |\mathbf{q}|$ at the Γ point.

We have discovered unusual singularities at T_c for $\mathbf{H} = \mathbf{0}$ and also at the critical magnetic field along $[111]$ direction, $H_c(111)$, and clarified their origin. One staggered quadrupole susceptibility shows a stronger divergence than conventional mean-field one, and more interestingly, one uniform quadrupole susceptibility also exhibits divergence, although the ordered phase is not ferro quadrupole one. This can partially explain the softening in the ultrasonic experiments, but for the complete understanding, we need further investigations.

We have also proposed that a possible origin of enhanced thermo-electric power in the high-field phase is related to this low-energy quadrupole excitation. This scenario is consistent with the fact that the position of Schottky peak of the specific heat $C(T)$ at high fields roughly coincides the peak position in the thermo-electric power.

As for possible inter-site couplings in the 1-2-20 compounds, we have shown that there exist various directional couplings. Important ones are the dipole-dipole interactions and dipole-octupole interactions. Quadrupole-phonon interactions are also presented and we have shown that the atoms at the 16c site should displace in a way determined by the quadrupole order pattern. This indicates that if the 1-2-20 system shows an antiferro quadrupole order, the inversion symmetry of the lattice structure should be broken at the same time, and as a result, the Dzyaloshinskii-Moriya interactions are induced. We have shown the form of the Dzyaloshinskii-Moriya vector in terms of the displacement at the 16c site. In the present paper, we have concentrated on analyzing a simple quadrupole-quadrupole model. For more quantitative comparison with experimental data, these interactions would be important.

In summary, we have investigated antiferro quadrupole order in Γ_3 non-Kramers doublet systems. We have pointed out that there is no pure O_2^2 antiferro quadrupole order from general arguments and the mean-field phase

diagram and excitation spectra have been demonstrated. We have also discovered unusual singularities at $T = T_c$ for $\mathbf{H} = \mathbf{0}$ and also the critical field along [111] direction. In the final part, we have presented a list of some nontrivial interactions in the 1-2-20 compounds, which would be important for further theoretical and experimental investigations.

Acknowledgement

The authors would thank K. Izawa, T. Onimaru, and T. Sakakibara for fruitful discussions. K. H. thanks H. Kusunose for his valuable comment on the CEF Hamiltonian. This work was supported by a Grant-in-Aid for Scientific Research (No. 30456199) from the Japan Society for the Promotion of Science.

Appendix A: Wavefunctions

In this Appendix, we list single-site wavefunctions classified by the irreducible representations in the T_d group used in this paper.

First, let us introduce notations. For Pr ions, a main configuration of f-electrons is the $J = 4$ multiplet and its nine levels split as $\Gamma_1 \oplus \Gamma_3 \oplus \Gamma_4 \oplus \Gamma_5$ due to H_{CEF} . Two components of Γ_3 doublet are denoted by $\{u, v\}$ and components of Γ_4 and Γ_5 triplets are written as $\{\tilde{X}, \tilde{Y}, \tilde{Z}\}$ and $\{X, Y, Z\}$, respectively. Representative forms for the irreducible representations in terms of spatial coordinates (x, y, z) are given as

$$u \sim 3z^2 - r^2, \quad v \sim \sqrt{3}(x^2 - y^2), \quad (\text{A}\cdot 1)$$

$$\tilde{X} \sim x(y^2 - z^2), \quad \tilde{Y} \sim y(z^2 - x^2), \quad \tilde{Z} \sim z(x^2 - y^2), \quad (\text{A}\cdot 2)$$

$$X \sim x, \quad Y \sim y, \quad Z \sim z, \quad (\text{A}\cdot 3)$$

where $r^2 = x^2 + y^2 + z^2$. Note that, in T_d symmetry, xyz belongs to Γ_1 , and thus, $x \sim yz$, $y \sim zx$, and $z \sim xy$. The spatial coordinate vector (x, y, z) is Γ_5 , while an angular momentum \mathbf{J} belongs to Γ_4 .

Using the above notations, the wavefunctions are given as

$$|\Gamma_1\rangle = \frac{1}{\sqrt{12}} \left[\sqrt{\frac{5}{2}}(|4\rangle + |-4\rangle) + \sqrt{7}|0\rangle \right], \quad (\text{A}\cdot 4)$$

$$|\Gamma_3 u\rangle = \frac{1}{\sqrt{12}} \left[\sqrt{\frac{7}{2}}(|4\rangle + |-4\rangle) - \sqrt{5}|0\rangle \right], \quad (\text{A}\cdot 5)$$

$$|\Gamma_3 v\rangle = \frac{1}{\sqrt{2}}(|2\rangle + |-2\rangle), \quad (\text{A}\cdot 6)$$

$$|\Gamma_4 \tilde{X}\rangle = \frac{1}{4i} \left[\sqrt{7}(|1\rangle + |-1\rangle) + (|3\rangle + |-3\rangle) \right], \quad (\text{A}\cdot 7)$$

$$|\Gamma_4 \tilde{Y}\rangle = -\frac{1}{4} \left[\sqrt{7}(|1\rangle - |-1\rangle) - (|3\rangle - |-3\rangle) \right], \quad (\text{A}\cdot 8)$$

$$|\Gamma_4 \tilde{Z}\rangle = \frac{1}{\sqrt{2}i}(|4\rangle - |-4\rangle), \quad (\text{A}\cdot 9)$$

$$|\Gamma_5 X\rangle = \frac{1}{4i} \left[(|1\rangle + |-1\rangle) - \sqrt{7}(|3\rangle + |-3\rangle) \right], \quad (\text{A}\cdot 10)$$

$$|\Gamma_5 Y\rangle = \frac{1}{4} \left[(|1\rangle - |-1\rangle) + \sqrt{7}(|3\rangle - |-3\rangle) \right], \quad (\text{A}\cdot 11)$$

$$|\Gamma_5 Z\rangle = \frac{1}{\sqrt{2}i}(|2\rangle - |-2\rangle). \quad (\text{A}\cdot 12)$$

Here, $|J_z\rangle$ is state with the z-component of the angular momentum J_z and $J = 4$.

Appendix B: Crystalline electric field Hamiltonian

Here, we comment on two representations of the local CEF Hamiltonian. The conventional representation is in terms of Stevens operators and it reads for $J = 4$ ion in CEF of T_d symmetry as

$$H_{\text{CEF}} = \sum_i \left\{ B_4^0 [O_4^0(i) + 5O_4^4(i)] + B_6^0 [O_6^0(i) - 21O_6^4(i)] \right\} \quad (\text{B}\cdot 1)$$

Here, O_n^m 's are the Stevens operators and B_n^m 's are constants.²⁵⁾ This form has been widely used to investigate CEF states in f-electron systems, but we have found that this is equivalent with the one represented by only two operators, and they are quadrupole moments defined as $Q_x = \sqrt{3}O_2^2/8$ and $Q_z = O_2^0/8$. This new representation is Eq. (1) shown in Sect. 2.1. Equation (1) explicitly shows the two invariances of Γ_3 quadrupole operators we consider. Apart from a trivial constant, Eq. (B.1) reduces to Eq. (1) and the parameters are related as

$$\epsilon_2 = \frac{640}{3}(B_4^0 - 126B_6^0), \quad \epsilon_3 = -\frac{78848}{9}B_6^0. \quad (\text{B}\cdot 2)$$

Appendix C: Mean-field ground-state energy for $\mathbf{H} = \mathbf{0}$

In this Appendix, we discuss the ground-state energy for $\mathbf{H} = \mathbf{0}$ on the basis of two-sublattice mean-field approximation. Since there are no matrix elements in the quadrupole operators between $\Gamma_{1,3}$ and $\Gamma_{4,5}$ states, the relevant Hilbert space here is spanned by Γ_3 and Γ_1 in our analysis.

First, let us show matrix forms of quadrupole operators in basis $\{|\Gamma_1\rangle, |\Gamma_3 u\rangle, |\Gamma_3 v\rangle\}$:

$$Q_z = \begin{pmatrix} 0 & a & 0 \\ a & 1 & 0 \\ 0 & 0 & -1 \end{pmatrix}, \quad Q_x = \begin{pmatrix} 0 & 0 & a \\ 0 & 0 & -1 \\ a & -1 & 0 \end{pmatrix} \quad (\text{C}\cdot 1)$$

where $a = \sqrt{35}/2$. The basis wavefunctions are explained in Appendix A.

We approximate the intersite interactions by a mean field of quadrupole $\mathbf{h} = -z\lambda\langle\mathbf{Q}\rangle = -\mathbf{q}$. Here, $\langle\mathbf{Q}\rangle$ is the thermal average on the nearest neighbor sites and z is the number of the nearest-neighbor sites. Thus, the mean-field Hamiltonian at one site is written as

$$H_{1\text{site}} = \begin{pmatrix} E_1 & aq_z & aq_x \\ aq_z & q_z & -q_x \\ aq_x & -q_x & -q_z \end{pmatrix}, \quad (\text{C}\cdot 2)$$

where $(q_z, q_x) = z\lambda(\langle Q_z \rangle, \langle Q_x \rangle) = q(\cos\theta, \sin\theta)$. The angle parameter is $0 \leq \theta < 2\pi$ and $q = \sqrt{q_z^2 + q_x^2}$. Let us first diagonalize the Γ_3 sector. This is done by using the following new basis:

$$|\Gamma_3+\rangle = \cos\frac{\theta}{2}|\Gamma_3u\rangle - \sin\frac{\theta}{2}|\Gamma_3v\rangle, \quad (\text{C.3})$$

$$|\Gamma_3-\rangle = \sin\frac{\theta}{2}|\Gamma_3u\rangle + \cos\frac{\theta}{2}|\Gamma_3v\rangle. \quad (\text{C.4})$$

Then, in terms of $\{|\Gamma_1\rangle, |\Gamma_3+\rangle, |\Gamma_3-\rangle\}$, H_{1site} reads as

$$H_{\text{1site}} = \begin{pmatrix} E_1 & aq \cos\frac{3\theta}{2} & aq \sin\frac{3\theta}{2} \\ aq \cos\frac{3\theta}{2} & q & 0 \\ aq \sin\frac{3\theta}{2} & 0 & -q \end{pmatrix}. \quad (\text{C.5})$$

We are interested in situation where $E_1 \gg z\lambda|\langle \mathbf{Q} \rangle| = q$ and obtain the ground-state energy of H_{1site} perturbatively as a series of the small parameter q/E_1 ,

$$\begin{aligned} \frac{E_{\text{1site}}^{\text{gs}}}{E_1} &= -\left(\frac{q}{E_1}\right) - \frac{35}{4}\left(\sin^2\frac{3\theta}{2}\right)\left(\frac{q}{E_1}\right)^2 \\ &+ \frac{35}{4}\left(\sin^2\frac{3\theta}{2} - \frac{35}{32}\sin^2 3\theta\right)\left(\frac{q}{E_1}\right)^3 + \dots \end{aligned} \quad (\text{C.6})$$

The mean-field ground-state energy for Eq. (4) is given per unit cell as

$$E_{\text{mf}}^{\text{gs}} = E_{\text{1site}}^{\text{gs}}(A) + E_{\text{1site}}^{\text{gs}}(B) - \frac{1}{z\lambda} \mathbf{q}^A \cdot \mathbf{q}^B, \quad (\text{C.7})$$

where $E_{\text{1site}}^{\text{gs}}(A)$ denotes the ground-state energy at A -site with q^A and θ_B , and similar definitions for the B -site.

Appendix D: Direct products of irreducible representations of T_d group

In this Appendix, we list a full set of reduction tables of direct products $\Gamma_i \otimes \Gamma_j$ in T_d point group. These are very useful for symmetry arguments to construct coupling constants with a given set of operators. The lists for $\Gamma_1 \otimes \Gamma_i$ and $\Gamma_2 \otimes \Gamma_i$ are not shown, since these are trivial. The others are as follows.

- $\Gamma_3 \otimes \Gamma'_3 = \Gamma_1 \oplus \Gamma_2 \oplus \Gamma_3$
 $\Gamma_1 : uu' + vv'$,
 $\Gamma_2 : uv' - vu'$,
 $\Gamma_3 : \{uu' - vv', -uv' - vu'\}$.
- $\Gamma_3 \otimes \Gamma_4 = \Gamma_4 \oplus \Gamma_5$
 $\Gamma_4 : \{(u - \sqrt{3}v)\tilde{X}, (u + \sqrt{3}v)\tilde{Y}, -2u\tilde{Z}\}$,
 $\Gamma_5 : \{(\sqrt{3}u + v)\tilde{X}, (-\sqrt{3}u + v)\tilde{Y}, -2v\tilde{Z}\}$.
- $\Gamma_3 \otimes \Gamma_5 = \Gamma_4 \oplus \Gamma_5$
 $\Gamma_4 : \{(\sqrt{3}u - v)X, (-\sqrt{3}u + v)Y, -2vZ\}$,
 $\Gamma_5 : \{(u - \sqrt{3}v)X, (u + \sqrt{3}v)Y, -2uZ\}$.
- $\Gamma_4 \otimes \Gamma'_4 = \Gamma_1 \oplus \Gamma_3 \oplus \Gamma_4 \oplus \Gamma_5$
 $\Gamma_1 : \tilde{X}\tilde{X}' + \tilde{Y}\tilde{Y}' + \tilde{Z}\tilde{Z}'$,
 $\Gamma_3 : \{2\tilde{Z}\tilde{Z}' - \tilde{X}\tilde{X}' - \tilde{Y}\tilde{Y}', \sqrt{3}(\tilde{X}\tilde{X}' - \tilde{Y}\tilde{Y}')\}$,

$$\begin{aligned} \Gamma_4 : &\{\tilde{Y}\tilde{Z}' - \tilde{Z}\tilde{Y}', \tilde{Z}\tilde{X}' - \tilde{X}\tilde{Z}', \tilde{X}\tilde{Y}' - \tilde{Y}\tilde{X}'\}, \\ \Gamma_5 : &\{\tilde{Y}\tilde{Z}' + \tilde{Z}\tilde{Y}', \tilde{Z}\tilde{X}' + \tilde{X}\tilde{Z}', \tilde{X}\tilde{Y}' + \tilde{Y}\tilde{X}'\}. \end{aligned}$$

- $\Gamma_4 \otimes \Gamma_5 = \Gamma_2 \oplus \Gamma_3 \oplus \Gamma_4 \oplus \Gamma_5$
 $\Gamma_2 : \tilde{X}X + \tilde{Y}Y + \tilde{Z}Z$,
 $\Gamma_3 : \{-\sqrt{3}(\tilde{X}X - \tilde{Y}Y), 2\tilde{Z}Z - \tilde{X}X - \tilde{Y}Y\}$,
 $\Gamma_4 : \{\tilde{Y}Z + \tilde{Z}Y, \tilde{Z}X + \tilde{X}Z, \tilde{X}Y + \tilde{Y}X\}$,
 $\Gamma_5 : \{\tilde{Y}Z - \tilde{Z}Y, \tilde{Z}X - \tilde{X}Z, \tilde{X}Y - \tilde{Y}X\}$.

- $\Gamma_5 \otimes \Gamma'_5 = \Gamma_1 \oplus \Gamma_3 \oplus \Gamma_4 \oplus \Gamma_5$
 $\Gamma_1 : XX' + YY' + ZZ'$,
 $\Gamma_3 : \{2ZZ' - XX' - YY', \sqrt{3}(XX' - YY')\}$,
 $\Gamma_4 : \{YZ' - ZY', ZX' - XZ', XY' - YX'\}$,
 $\Gamma_5 : \{YZ' + ZY', ZX' + XZ', XY' + YX'\}$.

Finally, we show a cubic invariant in the triple product $\Gamma_3 \otimes \Gamma'_3 \otimes \Gamma''_3$, which is directly related to Eq. (3):

- $\Gamma_3 \otimes \Gamma'_3 \otimes \Gamma''_3 = \Gamma_1 \oplus \Gamma_2 \oplus 3\Gamma_3$
 $\Gamma_1 : (uu' - vv')u'' - (uv' + vu')v''$,
 $\rightarrow u(u^2 - 3v^2)$ for $\Gamma_3 = \Gamma'_3 = \Gamma''_3$.

Appendix E: Landau free energy for quadrupole moment

To study quadrupole anisotropy, we will in this Appendix calculate the corresponding Landau free energy $F(\mathbf{Q})$ for a single site at magnetic field $\mathbf{H} = \mathbf{0}$, starting from the microscopic model. We first consider the case of finite temperature, and secondly study the zero-temperature case, which needs a special care.

We will calculate the quadrupole Landau free energy $F(\mathbf{Q})$ for a single site for a given temperature $T = \beta^{-1}$, with starting from the microscopic CEF Hamiltonian Eq. (1). To this end, we include to the Hamiltonian a coupling to conjugate field $\mathbf{h} = (h_z, h_x) = h(\cos\theta, \sin\theta)$ and obtain its related free energy $\tilde{F}(\mathbf{h})$:

$$\tilde{F}(\mathbf{h}) = -\frac{1}{\beta} \log \tilde{Z}(\mathbf{h}) = -\frac{1}{\beta} \log \text{Tr} e^{-\beta(H_{\text{CEF}} - \mathbf{h} \cdot \hat{\mathbf{Q}})}. \quad (\text{E.1})$$

The unperturbed Hamiltonian is a 9×9 matrix, and consists of the Γ_3 ground-state doublet and excited states, Γ_1 singlet and two triplets, Γ_4 and Γ_5 . With setting the ground-state energy zero $E_3 = 0$, the energies of these excited multiplets are denoted as E_1 , E_4 , and E_5 , respectively.

Using a standard technique, we first expand $\tilde{Z}(\mathbf{h})$ in h ,

$$\tilde{Z}(\mathbf{h}) = Z_0 + d_2 h^2 + d_3 h^3 + d_4 h^4 + \dots \quad (\text{E.2})$$

Here, the unperturbed partition function is $Z_0 = 2 + e^{-\beta E_1} + 3(e^{-\beta E_4} + e^{-\beta E_5})$. The first-order term vanishes, and this means that the thermal average of moment vanishes at any finite temperature, unless the inter-site interactions are switched on. It will turn out that the expansion up to the fourth order is sufficient for studying quadrupole anisotropy. Since the operators $\hat{\mathbf{Q}}$ are block-diagonal in the CEF bases in Appendix A, the expansion

is easy but the results are not so simple. The second- and the fourth-order terms are isotropic with respect to the field direction θ , while the third-order term depends as $\cos 3\theta$ and we denote $d_3 = \bar{d}_3 \cos 3\theta$. The explicit forms of $\{d_n\}$ are given as

$$\frac{d_2}{\beta^2} = 1 + \frac{35}{4} \frac{1 - e^{-\beta E_1}}{\beta E_1} + \frac{3}{16} (7^2 e^{-\beta E_4} + 2^2 e^{-\beta E_5}) + \frac{63}{32} \frac{e^{-\beta E_5} - e^{-\beta E_4}}{\beta(E_4 - E_5)}, \quad (\text{E.3})$$

$$\frac{\bar{d}_3}{\beta^3} = -\frac{35}{4} \left[\frac{1}{\beta E_1} - \frac{1 - e^{-\beta E_1}}{\beta^2 E_1^2} \right] - \frac{1}{27} \left[2(7^3 e^{-\beta E_4} - 8e^{-\beta E_5}) + 63 \frac{7e^{-\beta E_4} + 2e^{-\beta E_5}}{\beta(E_4 - E_5)} - 3^4 \cdot 7 \frac{e^{-\beta E_5} - e^{-\beta E_4}}{\beta^2(E_4 - E_5)^2} \right], \quad (\text{E.4})$$

$$\frac{d_4}{\beta^4} = \frac{1}{2^5 \cdot 3} \left[8 + 420 \frac{1}{\beta E_1} + 105 \frac{27 + 35e^{-\beta E_1}}{\beta^2 E_1^2} - 6510 \frac{1 - e^{-\beta E_1}}{\beta^3 E_1^3} \right] + \frac{3}{2^{10}} \left[(7^4 e^{-\beta E_4} + 2^4 e^{-\beta E_5}) + 21 \frac{7^2 e^{-\beta E_4} - 4e^{-\beta E_5}}{\beta(E_4 - E_5)} - \frac{3^3 \cdot 7 \cdot 7^2 e^{-\beta E_4} + 9e^{-\beta E_5}}{4 \beta^2(E_4 - E_5)^2} + \frac{9 \cdot 7 \cdot 29}{2} \frac{e^{-\beta E_5} - e^{-\beta E_4}}{\beta^2(E_4 - E_5)^2} \right]. \quad (\text{E.5})$$

Converting the moments $\{d_n\}$ into cumulants, the free energy is obtained as a series of h ,

$$\bar{F}(\mathbf{h}) \sim F_0 - \frac{1}{2} \chi h^2 - \frac{1}{3} \kappa_3 h_z (h_z^2 - 3h_x^2) + \frac{1}{4} \kappa_4 h^4, \quad (\text{E.6})$$

with $F_0 = -\beta^{-1} \log Z_0$ and the coefficients are

$$\chi = \frac{2}{\beta} \frac{d_2}{Z_0}, \quad \kappa_3 = \frac{3}{\beta} \frac{\bar{d}_3}{Z_0},$$

$$\kappa_4 = \frac{4}{\beta} \left[\frac{1}{2} \left(\frac{d_2}{Z_0} \right)^2 - \frac{d_4}{Z_0} \right] = \frac{\beta}{2} \chi^2 - \frac{4}{\beta} \frac{d_4}{Z_0}. \quad (\text{E.7})$$

The thermal average of the quadrupole moment is calculated as $\mathbf{Q} = (Q_z, Q_x) = Q(\cos \varphi, \sin \varphi) = -\partial \bar{F}(\mathbf{h}) / \partial \mathbf{h}$ and the result is

$$\mathbf{Q} \sim \chi \mathbf{h} + \kappa_3 h^2 (\cos 2\theta, -\sin 2\theta) - \kappa_4 h^2 \mathbf{h}. \quad (\text{E.8})$$

This shows that the second-order coefficient χ is the linear susceptibility of quadrupole and isotropic, and also that the third-order contribution tilts the moment away from the field direction.

The next step is to invert the relation and obtain for a given \mathbf{Q} its corresponding $\mathbf{h}(\mathbf{Q})$. This is easily done in the polar representation and the result is

$$h \sim \frac{Q}{\chi} - \frac{\kappa_3 Q^2}{\chi^3} \cos 3\varphi + \left[\frac{\kappa_3^2}{\chi^2} \left(1 + \frac{5}{2} \sin^2 3\varphi \right) + \frac{\kappa_4}{\chi} \right] \frac{Q^3}{\chi^3},$$

$$(\text{E.9})$$

$$\theta \sim \varphi + \frac{\kappa_3 Q}{\chi^2} \sin 3\varphi. \quad (\text{E.10})$$

Now, combining all these, we can obtain the Landau free energy of quadrupole moment. We perform the Legendre transformation, $F(\mathbf{Q}) = \bar{F}(\mathbf{h}(\mathbf{Q})) + \mathbf{Q} \cdot \mathbf{h}(\mathbf{Q})$ and obtain

$$F(\mathbf{Q}) \sim F_0 + \frac{1}{2\chi} Q^2 - \frac{\kappa_3}{3\chi^3} Q_z (Q_z^2 - 3Q_x^2) + \frac{1}{3\chi^5} (2\kappa_3^2 + \kappa_4 \chi) Q^4. \quad (\text{E.11})$$

As predicted by the symmetry argument, anisotropy is due to the third-order term.

With approaching zero temperature, the linear susceptibility diverges as $\chi \propto \beta = 1/T$. Therefore, all the coefficients in the expansion above vanish, since $\kappa_3 \propto \beta$ and $\kappa_4 \propto \beta^3$. This indicates that the expansion at zero temperature is not regular around $\mathbf{Q} = \mathbf{0}$. In the Γ_3 ground-state doublet, the modulus of quadrupole moment is $Q = 1$. Therefore, at zero temperature, we need expansion starting from $Q = 1$ not 0.

At zero temperature, it is sufficient to consider the ground states and the excited Γ_1 singlet. This is because Γ_1 is the only state that is connected to the ground state by matrix elements of $\hat{\mathbf{Q}}$. Solving the eigenvalue equation of the 3×3 Hamiltonian matrix, we obtain the exact ground state energy and its expansion in h reads

$$E_0(\mathbf{h}) \sim -h - \frac{35}{8E_1} h^2 \left[1 + \frac{h_z (h_z^2 - 3h_x^2)}{h^3} \right]. \quad (\text{E.12})$$

This result is different from the expansion of the free energy in two points. First, E_0 has the term of order h^1 . This implies the presence of spontaneous moment when the field \mathbf{h} is switched off. Secondly, the anisotropy appears in the order h^2 instead of h^3 , although the dependence on field direction is common with the finite-temperature case.

The quadrupole moment is again obtained by $\mathbf{Q} = -\partial E_0(\mathbf{h}) / \partial \mathbf{h}$ and the result in the polar representation is

$$Q \sim 1 + \frac{35}{2E_1} h \cos^2 \frac{3\theta}{2} + \frac{105^2}{27E_1^2} h^2 \sin^2 3\theta, \quad (\text{E.13})$$

$$\varphi \sim \theta - \frac{105}{8E_1} h \sin 3\theta. \quad (\text{E.14})$$

As we noted above, the quadrupole moment deviates from $Q = 1$ not 0 upon applying field at zero temperature. One should note that the correction terms vanish, when the field angle is $\theta = \frac{2}{3}\pi \times (\text{integer})$. This is also the case in the all orders in h . This is because the ground state does not change at all in this case upon increasing h .

The next step is the inversion of the relation $\mathbf{Q}(\mathbf{h})$ and

we get the field strength and angle as

$$\frac{h}{E_1} \sim \frac{Q-1}{\frac{35}{2} \cos^2 \frac{3}{2}\varphi} + \frac{945}{16} \left(\frac{Q-1}{\frac{35}{2} \cos^2 \frac{3}{2}\varphi} \right)^2 \sin^2 \frac{3}{2}\varphi, \quad (\text{E}\cdot 15)$$

$$\theta \sim \varphi + \frac{3}{2}(Q-1) \tan \frac{3}{2}\varphi. \quad (\text{E}\cdot 16)$$

Note that the small parameter in expansions is $(Q-1)/(\frac{35}{2} \cos^2 \frac{3}{2}\varphi)$.

Following the same procedure as for the Landau free energy at finite temperature, we obtain the zero-temperature energy of the quadrupole moment. The result is

$$\begin{aligned} \frac{E(\mathbf{Q})}{E_1} &\sim \frac{1}{35} \frac{(Q-1)^2}{\cos^2 \frac{3}{2}\varphi} \\ &- \frac{1}{70^2} \frac{(Q-1)^3}{\cos^4 \frac{3}{2}\varphi} \left(2547 - 2555 \cos^2 \frac{3}{2}\varphi \right). \quad (\text{E}\cdot 17) \end{aligned}$$

The zero-temperature result has two essential differences. First, the anisotropy starts to appear in the second order in $(Q-1)$, and secondly, the angle dependence is not a single harmonic like $\cos 3\varphi$. These two are evidences of the fact that the anisotropy at zero temperature cannot be represented by an analytic form in \mathbf{Q} , even if only small deviations are concerned.

Appendix F: Mean-field theory for susceptibility of a two-sublattice system

We explain in this Appendix a method of calculating susceptibility in a system with the two sublattices A and B . The input of the method is local susceptibility at one site of each sublattice, χ_{loc}^s ($s=A$ or B). We prepare its exact value by either an analytic or numerical method. This is easy since the local Hilbert space is small, nine dimensions in our case. Let us employ a mean-field theory and derive a formula that gives the susceptibility of the entire system from the local susceptibilities. To be specific, we will consider the response of quadrupole moment \mathbf{Q}^s with respect to its conjugate field \mathbf{h}^s .

In the mean-field theory, quadrupole moment at each site feels an effective field that consists of the molecular fields contributed by its neighbor sites and an external conjugate field. This is represented by the following mean-field Hamiltonian

$$H_{\text{MF}}^s = H_{\text{loc}}^s - (\mathbf{h}^s - g\langle \mathbf{Q}^{\bar{s}} \rangle) \cdot \mathbf{Q}^s = H_0^s - \mathbf{h}^s \cdot \mathbf{Q}^s. \quad (\text{F}\cdot 1)$$

Here, the intersite coupling is $g = z\lambda$ and $s = A$ or B with $\bar{A} = B$ and vice versa. The on-site part H_{loc}^s is the CEF Hamiltonian H_{CEF} plus the Zeeman coupling to magnetic field if it is applied. It does not matter if the magnetic field depends on the sublattices or not, and the following results hold. H_0^s is the unperturbed part, when concerned is the linear response to *external fields* $\mathbf{h}^{A,B}$, and this already includes the contribution of the molecular fields in ordered phases.

Now, let us examine the linear response of \mathbf{Q} at each

sublattice. There are two points. The first is that the susceptibility is a 2×2 matrix in \mathbf{Q} space and also a 2×2 matrix in the sublattice space

$$\delta Q_\mu^s = \sum_{s,\mu'} \chi_{\mu\mu'}^{ss'} h_{\mu'}^{s'}. \quad (\text{F}\cdot 2)$$

Here, δQ_μ^s denote the induced moments due to the external fields, and we will calculate $\chi_{\mu\mu'}^{ss'}$. The second point is important and the core idea of the mean-field theory: the induced moments modifies the molecular fields, and this can be represented by the renormalization of the external fields. Since we know exactly the local response at each sublattice, they constitute self-consistency conditions

$$\delta \mathbf{Q}^s = \underline{\chi}_{\text{loc}}^s (\mathbf{h}^s - g\delta \mathbf{Q}^{\bar{s}}). \quad (\text{F}\cdot 3)$$

Here, under-bar denotes a 2×2 matrix, and the orbital-space degrees of freedom are thus represented by vector and matrix for simplicity.

It is straightforward to solve these and we obtain

$$\underline{\chi}^{ss} = (\underline{1} - g^2 \underline{\chi}_{\text{loc}}^s \underline{\chi}_{\text{loc}}^{\bar{s}})^{-1} \underline{\chi}_{\text{loc}}^s, \quad (\text{F}\cdot 4)$$

$$\underline{\chi}^{s\bar{s}} = -g(\underline{1} - g^2 \underline{\chi}_{\text{loc}}^s \underline{\chi}_{\text{loc}}^{\bar{s}})^{-1} \underline{\chi}_{\text{loc}}^s \underline{\chi}_{\text{loc}}^{\bar{s}}. \quad (\text{F}\cdot 5)$$

The uniform and staggered susceptibilities are given as

$$\underline{\chi}^\pm = \underline{\chi}^{AA} + \underline{\chi}^{BB} \pm (\underline{\chi}^{AB} + \underline{\chi}^{BA}), \quad (\text{F}\cdot 6)$$

$$= \sum_{s=A,B} (\underline{1} - g^2 \underline{\chi}_{\text{loc}}^s \underline{\chi}_{\text{loc}}^{\bar{s}})^{-1} \underline{\chi}_{\text{loc}}^s (\underline{1} \mp g \underline{\chi}_{\text{loc}}^{\bar{s}}). \quad (\text{F}\cdot 7)$$

If a staggered order is present, it induces the cross responses

$$\underline{\chi}^{+-}, \underline{\chi}^{-+} = \underline{\chi}^{AA} - \underline{\chi}^{BB} \mp (\underline{\chi}^{AB} - \underline{\chi}^{BA}). \quad (\text{F}\cdot 8)$$

Here, $\underline{\chi}^{+-}$ and $\underline{\chi}^{-+}$ take $-$ and $+$ sign, respectively. Beware that these are not symmetric in the internal \mathbf{Q} space, and the correct symmetry is $(\underline{\chi}^{+-})_{\mu\mu'} = (\underline{\chi}^{-+})_{\mu'\mu}$.

Appendix G: Landau theory of antiferro quadrupole order

In this Appendix, we study the Landau free energy for the antiferro quadrupole order and find its minimum point. As discussed in details in Appendix E, the single-site free energy is given by Eq. (E.11). Adding the intersite interaction, we set up a minimal form of the total free energy

$$\begin{aligned} F_{\text{tot}} &= \sum_{s=A,B} \left[\frac{1}{2} a |\mathbf{Q}^s|^2 - \frac{1}{3} \gamma Q_z^s (Q_z^{s2} - 3Q_x^{s2}) \right. \\ &\quad \left. + \frac{1}{4} b |\mathbf{Q}^s|^4 \right] + g \mathbf{Q}^A \cdot \mathbf{Q}^B. \quad (\text{G}\cdot 1) \end{aligned}$$

Here, a, b, γ , and g are all positive phenomenological constants and we will consider the transition with the change of a . This free energy (G.1) is appropriate for $\mathbf{H} = \mathbf{0}$ and also for $\mathbf{H} \parallel [111]$, where the magnetic field does not di-

rectly couple with \mathbf{Q} . Note that F_{tot} is invariant upon simultaneous rotation of $\mathbf{Q}^{A,B}$ by the angle $\pm\frac{2}{3}\pi$, but not invariant for inversion $\mathbf{Q}^{A,B} \rightarrow -\mathbf{Q}^{A,B}$ due to the γ term.

For simplicity, we focus on the case of $|\mathbf{Q}^A| = |\mathbf{Q}^B|$. This corresponds to the mean-field solutions for $\mathbf{H} = \mathbf{0}$ and $\mathbf{H} \parallel [111]$. Parameterizing $\mathbf{Q}^s = (Q_z^s, Q_x^s) = q(\cos\theta_s, \sin\theta_s)$, the free energy is now a function of the two angles and the common amplitude

$$F_{\text{tot}} = aq^2 + \frac{1}{2}bq^4 + gq^2R(\theta_A, \theta_B). \quad (\text{G}\cdot 2)$$

Here, the new factor is

$$R(\theta_A, \theta_B) \equiv \cos(\theta_A - \theta_B) - \frac{\gamma}{3g}q(\cos 3\theta_A + \cos 3\theta_B). \quad (\text{G}\cdot 3)$$

We minimize F_{tot} in two steps; we first minimize R for a given q and secondly minimize the whole with respect to q . R is minimized for a nearly antiparallel configuration of the two quadrupole moments;

$$\theta_{A,B} = \pm \left(\frac{\pi}{2} + \frac{\gamma}{2g}q \right), \quad R_{\text{min}} \sim -1 - \frac{\gamma^2}{2g^2}q^2. \quad (\text{G}\cdot 4)$$

There are two other solutions, but they agree to the above one by symmetry operation of $\pm 2\pi/3$ rotation.

Inserting this result to Eq. (G·2), we find the function to be minimized is a standard ϕ^4 -model with modified coefficients

$$F_{\text{tot}} \sim \tilde{a}q^2 + \frac{1}{2}\tilde{b}q^4, \quad \tilde{a} \equiv a - g, \text{ and } \tilde{b} \equiv b - \gamma^2/g. \quad (\text{G}\cdot 5)$$

Here, $\tilde{b} > 0$ if the anisotropy is not so strong, and we first consider this case. Then, the transition is continuous. Finite moments start to appear when a becomes smaller than the critical value $a_c = g$, and their amplitude is the mean-field result of the ϕ^4 -model, $q \sim (|\tilde{a}|/\tilde{b})^{1/2}$. Including higher-order corrections in the calculations above, we obtain the result up to the next order

$$q \sim \sqrt{\frac{|\tilde{a}|}{\tilde{b}}} \left(1 - \frac{\gamma^4}{2\tilde{b}^2g^3}|\tilde{a}| \right). \quad (\text{G}\cdot 6)$$

In the case of this continuous transition, the angle between $\mathbf{Q}^{A,B}$ starts from π and gradually deforms with the growth of their amplitude as shown by Eq. (G·4).

When the anisotropy is strong $\tilde{b} < 0$, we need to include the next-order term in q ,

$$F_{\text{tot}} \sim \tilde{a}q^2 + \frac{1}{2}\tilde{b}q^4 + \frac{\gamma^2}{3g}q^6. \quad (\text{G}\cdot 7)$$

This is the ϕ^6 -model and describes a first-order transition upon varying a , when $\tilde{b} < 0$. This transition takes place at

$$a_{\#} \sim g \left(1 + \frac{3\tilde{b}^2g^2}{16\gamma^4} \right) > a_c, \quad (\text{G}\cdot 8)$$

and there the order parameter jumps to

$$\bar{q}_{\#} \sim \sqrt{\frac{3|\tilde{b}|g^3}{4\gamma^4}}. \quad (\text{G}\cdot 9)$$

Note that in the case that the moments $\mathbf{Q}^{A,B}$ are not completely antiparallel at the transition point,

$$\Delta\theta \equiv \theta_A - \theta_B - \pi \sim \sqrt{\frac{3|\tilde{b}|g}{4\gamma^2}}. \quad (\text{G}\cdot 10)$$

Even when the anisotropy is very strong, the result (G·9) is still valid, but the angle deformation approaches $\Delta\theta \rightarrow \frac{1}{3}\pi$.

Appendix H: How to make invariant form

In this Appendix, we will discuss a general method to construct interactions that are invariant under a given point group. Although the following discussion is essentially the same as that done by Sakai *et al.*,³⁸⁾ we show some details of the calculations.

Let us consider site i and its nearest neighbor sites $j = 1, 2, 3$, and 4 in a diamond lattice structure. The relative positions of the nearest neighbors ($j = 1, 2, 3$, and 4) are $(111)/4$, $(\bar{1}\bar{1}\bar{1})/4$, $(1\bar{1}\bar{1})/4$, and $(\bar{1}\bar{1}1)/4$ for $j = 1, 2, 3, 4$, respectively, where we set the lattice constant to unity. See, Fig. 19. A general form of interactions between the nearest-neighbors is

$$V_i = \sum_{\mu\nu} \sum_j \lambda_j^{\mu\nu} A_i^{\mu} B_j^{\nu}. \quad (\text{H}\cdot 1)$$

Here, $\lambda_j^{\mu\nu}$ is the coupling constant and $A^{\mu}(B^{\nu})$ transforms as one of the irreducible representations $\mu(\nu)$ for local T_d point group without changing the site index. We represent the local point group operation by R_{loc} and also symmetry operation around the i site on the site index j by R_{site} .

Now, we change the representations μ and ν , which are not irreducible with respect to the index of irreducible representation for $A \otimes B$. We denote this index as l and Eq. (H·1) is now given as

$$V_i = \sum_{j=1}^4 \sum_l \lambda_j^l [A_i \otimes B_j]_l \equiv \sum_{j=1}^4 \sum_l \lambda_j^l C_{ijl}. \quad (\text{H}\cdot 2)$$

This is further symmetrized by taking a following representation instead of j :

$$V_i = \sum_l \lambda_s^l C_{il}^s + \sum_l \bar{\lambda}^l \cdot \bar{C}_{il}, \quad (\text{H}\cdot 3)$$

$$\lambda_s^l = \frac{1}{2} \sum_{j=1}^4 \lambda_j^l, \quad \lambda_x^l = \frac{1}{2}(\lambda_1^l - \lambda_2^l + \lambda_3^l - \lambda_4^l), \quad (\text{H}\cdot 4)$$

$$\lambda_y^l = \frac{1}{2}(\lambda_1^l - \lambda_2^l - \lambda_3^l + \lambda_4^l), \quad \lambda_z^l = \frac{1}{2}(\lambda_1^l + \lambda_2^l - \lambda_3^l - \lambda_4^l). \quad (\text{H}\cdot 5)$$

Note that

$$(\vec{\lambda}^l)_u = \sum_{j=1}^4 \hat{U}_{uj} \lambda_j^l = \frac{\sqrt{3}}{2} \sum_{j=1}^4 (\hat{r}_{ji})_u \lambda_j^l, \quad (\text{H}\cdot 6)$$

where \hat{r}_{ji} is the unit vector to j from i , and similar definitions for C_{il}^s and $(\vec{C}_{il})_u = \sum_j \hat{U}_{uj} C_{ijl}$. The site indices of C_{il}^s transform as Γ_1 under the operations R_{site} , while that of \vec{C}_{il} as Γ_5 and λ 's do not transform under symmetry operations R_{site} because they are just coupling constants. Since under the operations R_{loc} , different irreducible representations in l do not mix, we can analyze $l \in \Gamma_1, \Gamma_2, \Gamma_3, \Gamma_4$ and Γ_5 , separately. The result is very simple and there are only two couplings: $\lambda_s^{\Gamma_1}$ and $\vec{\lambda}^{\Gamma_5}$. The latter is given by $\vec{\lambda}^X = \lambda^{\Gamma_5}(1, 0, 0)$, $\vec{\lambda}^Y = \lambda^{\Gamma_5}(0, 1, 0)$, $\vec{\lambda}^Z = \lambda^{\Gamma_5}(0, 0, 1)$, leading to

$$V_i = \lambda_s^{\Gamma_1} \sum_{j=1}^4 C_{ij\Gamma_1} + \lambda^{\Gamma_5} \sum_{j=1}^4 \hat{r}_{ji} \cdot \begin{pmatrix} C_{ijX} \\ C_{ijY} \\ C_{ijZ} \end{pmatrix}. \quad (\text{H}\cdot 7)$$

Equation (H·7) indicates that we need to construct Γ_1 or Γ_5 representations by a given set of operators A and B . Finally, since the above derivation does not include the fact that the bond center of the diamond lattice structure is the inversion center of the system, interactions obtained should be symmetrized with respect to the inversion operations. Even when the number of operators included increases, the above discussion is still valid by regarding $C_{ijl} = [A_i \otimes A'_i \otimes \cdots \otimes B_j \otimes B'_j \otimes \cdots]_l$.

- 1) Y. Tokura and N. Nagaosa, *Science*, **288**, 462 (2000).
- 2) Y. Kuramoto, H. Kusunose, and A. Kiss, *J. Phys. Soc. Jpn.* **78**, 072001 (2009).
- 3) T. Onimaru, K. T. Matsumoto, Y. F. Inoue, K. Umeo, Y. Saiga, Y. Matsushita, R. Tamura, K. Nishimoto, I. Ishii, T. Suzuki, and T. Takabatake, *J. Phys. Soc. Jpn.* **79**, 033704 (2010).
- 4) T. Onimaru, K. T. Matsumoto, Y. F. Inoue, K. Umeo, T. Sakakibara, Y. Karaki, M. Kubota, and T. Takabatake, *Phys. Rev. Lett.* **106**, 177001 (2011).
- 5) T. Onimaru, N. Nagasawa, K. T. Matsumoto, K. Wakiya, K. Umeo, S. Kittaka, T. Sakakibara, Y. Matsushita, and T. Takabatake, *Phys. Rev. B* **86**, 184426 (2012).
- 6) A. Sakai and S. Nakatsuji, *J. Phys. Soc. Jpn.* **80**, 063701 (2011).
- 7) A. Sakai, K. Kuga, and S. Nakatsuji, *J. Phys. Soc. Jpn.* **81**, 083702 (2012).
- 8) K. Matsubayashi, T. Tanaka, A. Sakai, S. Nakatsuji, Y. Kubo, and Y. Uwatoko, *Phys. Rev. Lett.* **109**, 187004 (2012).
- 9) Y. Shimura, Y. Ohta, T. Sakakibara, A. Sakai, and S. Nakatsuji, *J. Phys. Soc. Jpn.* **82**, 043705 (2013).
- 10) I. Ishii, H. Muneshige, Y. Suetomi, T. K. Fujita, T. Onimaru, K. T. Matsumoto, T. Takabatake, K. Araki, M. Akatsu, Y. Nemoto, T. Goto, and T. Suzuki, *J. Phys. Soc. Jpn.* **80**, 093601 (2011).
- 11) I. Ishii, H. Muneshige, S. Kamikawa, T. K. Fujita, T. Onimaru, N. Nagasawa, T. Takabatake, and T. Suzuki, *Phys. Rev. B* **87**, 205106 (2013).

- 12) M. Matsushita, J. Sakaguchi, Y. Taga, M. Ohya, S. Yoshiuchi, H. Ota, Y. Hirose, K. Enoki, F. Honda, K. Sugiyama, M. Hagiwara, K. Kindo, T. Tanaka, Y. Kubo, T. Takeuchi, R. Settai, and Y. Ōnuki, *J. Phys. Soc. Jpn.* **80**, 074605 (2011).
- 13) K. Iwasa, H. Kobayashi, T. Onimaru, K. T. Matsumoto, N. Nagasawa, T. Takabatake, S. O. Kawamura, T. Kikuchi, Y. Inamura, and K. Nakajima, *J. Phys. Soc. Jpn.* **82**, 043707 (2013).
- 14) T. J. Sato, S. Ibuka, Y. Nambu, T. Yamazaki, T. Hong, A. Sakai, and S. Nakatsuji, *Phys. Rev. B* **86**, 184419 (2012).
- 15) T. Inui, Y. Tanabe, and Y. Onodera, *Group Theory and Its Applications in Physics* (Springer-Verlag, Berlin, 1990).
- 16) R. Shiina, H. Shiba, and P. Thalmeier, *J. Phys. Soc. Jpn.* **66**, 1741 (1997).
- 17) P. Thalmeier, R. Shiina, H. Shiba, and O. Sakai, *J. Phys. Soc. Jpn.* **67**, 2363 (1998).
- 18) T. Matsumura, S. Nakamura, T. Goto, H. Amitsuka, K. Matsuhira, T. Sakakibara, and T. Suzuki, *J. Phys. Soc. Jpn.* **67**, 612 (1998).
- 19) R. Shiina, H. Shiba, and O. Sakai, *J. Phys. Soc. Jpn.* **68**, 2105 (1999).
- 20) P. Morin, D. Schmitt and E. du Tremolet de Lacheisserie, *J. Magn. Magn. Mater.* **30**, 257 (1982).
- 21) A. Yatskar, W. P. Beyermann, R. Movshovich, and P. C. Canfield, *Phys. Rev. Lett.* **77**, 3637 (1996).
- 22) H. Tanida, H. S. Suzuki, S. Takagi, H. Onodera and K. Tanigaki, *J. Phys. Soc. Jpn.* **75**, 073705 (2006).
- 23) T. Tayama, T. Sakakibara, K. Kitami, M. Yokayama, K. Tenya, H. Amitsuka, D. Aoki, Y. Ōnuki, Z. Kletowski, *J. Phys. Soc. Jpn.* **70**, 248 (2001).
- 24) T. Onimaru, private communication.
- 25) K. W. H. Stevens, *Proc. Phys. Soc., Sect. A* **65**, 209 (1952).
- 26) We also note that CEF potential due to T_h symmetry $O_6^2 - O_6^6$, which makes the Γ_4 and Γ_5 states in the T_d (and also O_h) symmetry hybridized, can be represented also by the quadrupole operators as

$$O_6^2(i) - O_6^6(i) \propto Q_x^3(i) - 3\overline{Q_x(i)Q_z^2(i)} \rightarrow -Q^3(i) \sin 3\theta(i). \quad (\text{H}\cdot 8)$$
- 27) When the anisotropy is infinitely strong, the model would reduce to antiferro magnetic 3-state Potts model. A classical Monte Carlo simulation of this model on the diamond lattice indicates that the criticality belongs to 3 dimensional XY universality class: S. Lapinskas and A. Rosengren, *Phys. Rev. Lett.* **81**, 1302 (1998).
- 28) M. Koseki, Y. Nakanishi, K. Deto, G. Koseki, R. Kashiwazaki, F. Shichinomiya, M. Nakamura, M. Yoshizawa, A. Sakai, and S. Nakatsuji, *J. Phys. Soc. Jpn.* **80**, SA049 (2011).
- 29) A. Joshi, M. Ma, F. Mila, D. N. Shi, and F. C. Zhang, *Phys. Rev. B* **60**, 6584 (1999).
- 30) H. Kusunose and Y. Kuramoto, *J. Phys. Soc. Jpn.* **70**, 3076 (2001).
- 31) L. D. Landau and E. M. Lifshitz, *Statistical Physics* (Pergamon Press, Oxford, 1959) Part 1.
- 32) P. M. Levy, *J. Phys. C* **6**, 3545 (1973).
- 33) K. Izawa, private communication.
- 34) T. Onimaru, private communication.
- 35) M. Lavagna, C. Lacroix, and M. Cyrot, *Phys. Letter* **89A**, 154 (1982).
- 36) V. Zlatić and R. Monnier, *Phys. Rev. B* **71**, 165109 (2005).
- 37) T. Hasegawa, N. Ogita, and M. Udagawa, *J. Phys. Conf. Seri.* **391**, 012016 (2012).
- 38) O. Sakai, R. Shiina, and H. Shiba, *J. Phys. Soc. Jpn.* **72**, 1534 (2003).